

1 **Investigation of post-depositional processing of nitrate in East**
2 **Antarctic snow: Isotopic constraints on photolytic loss, re-oxidation,**
3 **and source inputs**

4 **Short title:** Isotopes of nitrate in East Antarctic snow

5
6 G. Shi^{1,2}, A. M. Buffen², M. G. Hastings², C. Li³, H. Ma¹, Y. Li¹, B. Sun¹, C. An¹, S.
7 Jiang¹

8
9 ¹Key Laboratory for Polar Science of State Oceanic Administration, Polar Research
10 Institute of China, Shanghai 200062, China

11 ²Department of Earth, Environmental and Planetary Sciences and Institute at Brown for
12 Environment and Society, Brown University, Providence, Rhode Island 02912, USA.

13 ³The State Key Laboratory of the Cryospheric Sciences, Cold and Arid Regions
14 Environmental and Engineering Research Institute, Chinese Academy of
15 Sciences, Lanzhou 730000, China

16

17 **Correspondence to: M.G. Hastings (meredith_hastings@brown.edu)**

18

19

20 **Abstract**

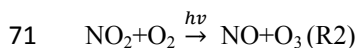
21 Snowpits along a traverse from coastal East Antarctica to the summit of the ice sheet (Dome Argus) are used
22 to investigate the post-depositional processing of nitrate in snow. Seven snowpits from sites with
23 accumulation rates between 24 and 172 kg m⁻² a⁻¹ were sampled to depths of 150 to 300 cm. At sites from
24 the continental interior (low accumulation, <55 kg m⁻² a⁻¹), nitrate mass fraction is generally >200 ng g⁻¹ in
25 surface snow and decreases quickly with depth to <50 ng g⁻¹. Considerably increasing values of δ¹⁵N of
26 nitrate are also observed (16-461‰ vs. air N₂), particularly in the top 20 cm, which is consistent with
27 predicted fractionation constants for the photolysis of nitrate. The δ¹⁸O of nitrate (17-84‰ vs. VSMOW), on
28 the other hand, decreases with increasing δ¹⁵N, suggestive of secondary formation of nitrate in situ
29 (following photolysis) with a low δ¹⁸O source. Previous studies have suggested that δ¹⁵N and δ¹⁸O of nitrate
30 at deeper snow depths should be predictable based upon an exponential decrease derived near the surface. At
31 deeper depths sampled in this study, however, the relationship between nitrate mass fraction and δ¹⁸O
32 changes, with increasing δ¹⁸O of nitrate observed between 100-200cm. Predicting the impact of
33 post-depositional loss, and therefore changes in the isotopes with depth, is highly sensitive to the depth
34 interval over which an exponential decrease is assumed. In the snowpits collected closer to the coast
35 (accumulation >91 kg m⁻² a⁻¹), there are no obvious trends detected with depth and instead seasonality in
36 nitrate mass fraction and its isotopic composition is found. In comparison to the interior sites, the coastal
37 pits are lower in δ¹⁵N (-15-71‰ vs. air N₂) and higher in δ¹⁸O of nitrate (53-111‰ vs. VSMOW). The
38 relationships found amongst mass fraction, δ¹⁵N, δ¹⁸O and Δ¹⁷O (Δ¹⁷O = δ¹⁷O – 0.52×δ¹⁸O) of nitrate cannot
39 be explained by local post-depositional processes, and are instead interpreted in the context of a primary
40 atmospheric signal. Consistent with other Antarctic observational and modeling studies, the isotopic results
41 are suggestive of an important influence of stratospheric chemistry on nitrate formation during the cold
42 season and a mix of tropospheric sources and chemistry during the warm season. Overall, the findings in
43 this study speak to the sensitivity of nitrate isotopic composition to post-depositional processing and
44 highlight the strength of combined use of the nitrogen and oxygen isotopes for a mechanistic understanding
45 of this processing.

46
47
48
49
50
51
52
53
54
55
56
57
58
59
60
61
62
63

64 **1 Introduction**

65

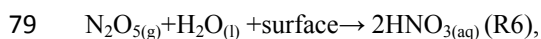
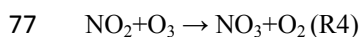
66 Nitrate (NO_3^-) is one of the major ions measured in Antarctic snow and ice. In the atmosphere, NO_3^- is
67 formed by oxidation of NO and NO_2 , which are collectively referred to as NO_x . In the presence of sunlight,
68 NO and NO_2 recycle rapidly with ozone (O_3), peroxy radical (HO_2), an organic radical (RO_2 , where
69 R=organics), or halogen radicals (XO , where X=Br, Cl or I) according to the following reactions:



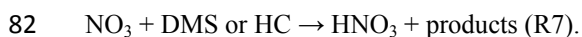
72 During the day, i.e., when sunlight is present, oxidation of NO_2 by the hydroxyl radical (OH) produces nitric
73 acid (HNO_3):



75 At night and in colder environments, oxidation of NO_2 by O_3 is promoted and HNO_3 can be formed from
76 hydrolysis of dinitrogen pentoxide (N_2O_5),



80 or by abstraction of a hydrogen atom by the nitrate radical (NO_3) from dimethyl sulfide (DMS) or a
81 hydrocarbon (HC),



83 Important NO_x inputs to the troposphere include fossil fuel combustion, biomass burning, soil microbial
84 activity, lightning, and injection from the stratosphere (Delmas et al., 1997; Lee et al., 1997). There has been
85 interest in using ice core NO_3^- records to reconstruct past atmospheric NO_x sources, and atmospheric
86 loading and variability in concentration over time. Increasing NO_3^- concentrations in Greenland ice core
87 records has been linked to increasing anthropogenic emissions (fossil fuel and/or agricultural) since the
88 Industrial Revolution (Mayewski and Legrand, 1990; Hastings et al., 2009). In contrast, such increases in
89 NO_3^- have not been observed in Antarctica (Wolff, 1995; Wolff et al., 2012), suggesting that concentrations
90 in snow are mainly controlled by natural sources.

91 The partitioning of NO_x inputs using ice core NO_3^- concentrations is difficult, however, since
92 concentration alone cannot identify specific NO_x sources and NO_3^- can be lost from snow by
93 post-depositional processes such as photolysis and possibly volatilization as HNO_3 (Wolff, 1995;
94 Röthlisberger et al., 2000; Frey et al., 2009). Measurements of nitrogen and oxygen stable isotope ratios in
95 NO_3^- provide further constraints for past NO_x sources and oxidation chemistry (Alexander et al., 2004;
96 Hastings et al., 2009; Hastings, 2010). In the atmosphere, the oxygen isotopes in NO_3^- reflect the oxidants
97 involved in the production of NO_3^- (e.g., R1-R7 above; Hastings et al., 2003; Michalski et al., 2003;
98 Alexander et al., 2009), and the nitrogen isotopes can reflect NO_x sources and possible imprints of transport
99 and chemistry (Hastings et al., 2003; Elliott et al., 2007; Savarino et al., 2007; Morin et al., 2008; Altieri et
100 al., 2013). However, post-depositional processing in snow can modify the isotopic composition of NO_3^- . At
101 Dome C in East Antarctica (where the snow accumulation rate is roughly $25 \text{ kg m}^{-2} \text{ a}^{-1}$, i.e., $<10 \text{ cm snow}$
102 a^{-1}), NO_3^- mass fractions decrease from hundreds of ng g^{-1} in surface snow to tens of ng g^{-1} at a depth of
103 10cm and this decrease corresponds to large changes in isotopic composition (Röthlisberger et al., 2000;
104 Blunier et al., 2005; Frey et al., 2009; Erbland et al., 2013) such that this processing should be identifiable
105 where it occurs. The influence of post-depositional alteration on NO_3^- , however, appears closely related to
106 annual snow accumulation and at sites with higher accumulation rates, such as Summit, Greenland (200 kg

107 $\text{m}^{-2} \text{a}^{-1}$, i.e., $\approx 60 \text{ cm snow a}^{-1}$; Dibb and Fahnstock, 2004), the post-depositional effects are rather minor,
108 and the atmospheric signal appears to be preserved (Hastings et al., 2004; Fibiger et al., 2013 and references
109 therein).

110 In recent studies, the spatial variability of photolytic and volatile NO_3^- loss in East Antarctic upper snow
111 has been investigated (Frey et al., 2009; Erbland et al., 2013), and represents important progress in
112 understanding air-snow transfer of NO_3^- . However, there are still a number of questions regarding the
113 interpretation of NO_3^- isotopes due to the complicated post-depositional behavior of NO_3^- . Distinguishing
114 the form, extent and relative importance of the different possible isotope effects associated with
115 post-depositional processes is critical for understanding what NO_3^- in an ice core represents.

116 In this study, samples from 150 to 300 cm-deep snowpits, have been collected at seven sites along a
117 traverse from the East Antarctic coast to Dome Argus (Dome A: the summit of the Antarctic ice sheet), and
118 NO_3^- mass fraction and isotopic composition were determined. The key objectives of this study are: (1) to
119 investigate the effects of post-depositional processes on isotopic composition of NO_3^- at different depths in
120 the snowpack; and (2) to understand the variation of NO_3^- isotopes in different environments across the East
121 Antarctic Ice Sheet (EAIS). The results of this study are of significance to a further understanding of
122 post-depositional processing of snow NO_3^- and the interpretation of NO_3^- isotopic composition archived in
123 ice cores.

124

125 **2 Materials and methods**

126

127 **2.1 Sample collection**

128

129 The Chinese National Antarctic Research Expedition (CHINARE) team conducts an annual inland
130 traverse from the coastal Zhongshan Station (Indian Ocean sector) to Dome A in East Antarctica (Fig. 1).
131 This traverse covers a distance of 1250 km. On the traverse route from Zhongshan to Dome A, seven
132 snowpits were excavated during the 2012/2013 austral summer season (Fig. 1). Full information about each
133 pit, including location, snow depth, sampling resolution, collection date, mean annual snow accumulation,
134 etc., is summarized in Table 1.

135 Snowpits were excavated manually and one snow wall was scraped clean and flat with a high-density
136 polyethylene (HDPE) scraper. Snow samples were collected using 250ml narrow-mouth HDPE vials pushed
137 horizontally into the snow wall beginning at the bottom of the pit and moving upwards. The scraper and
138 vials were pre-cleaned with Milli-Q ultrapure water ($>18.2 \text{ M}\Omega$), dried in a class 100 super clean hood at 20
139 $^{\circ}\text{C}$ and then sealed in the clean polyethylene (PE) bags that were not opened until the field sampling started.
140 Field blanks consisting of sampling bottles filled with Milli-Q water were analyzed for ion concentrations.
141 All personnel wore PE gloves and face masks and the pit sites were generally 1 km away from the traverse
142 route to avoid possible contamination from expedition team activities. After collection, the vials were again
143 sealed in clean PE bags and preserved in a clean insulated cabinet. All together, 530 snow samples were
144 collected. All samples were transported to China in a freezer at -25°C and then shipped frozen to Brown
145 University in Providence, RI.

146

147 **2.2 Sample analysis**

148

149 Snow NO_3^- mass fractions (denoted as $w(\text{NO}_3^-)$ in the following context) were determined using a Westco
150 Scientific SmartChem 200 discrete chemistry analyzer. The SD (standard deviation) of $w(\text{NO}_3^-)$ of 55 field

151 blanks run within sets of samples was 0.8 ng g^{-1} , which is comparable to blank Milli-Q water run on the
152 same system. The pooled standard deviation of samples run in replicate ($n=50$) in different sample sets is
153 1.5 ng g^{-1} .

154 Snow NO_3^- isotopic compositions were measured according to the denitrifier method by using
155 denitrifying bacteria to convert NO_3^- to N_2O gas, which is collected and injected into a stable isotope ratio
156 mass spectrometer (Thermo Scientific DELTA V Plus; Sigman et al., 2001; Casciotti et al., 2002; Kaiser et
157 al., 2007). At Brown, a minimum of 5 nmol of NO_3^- is required for an accurate isotopic determination of
158 $^{15}\text{N}/^{14}\text{N}$ and $^{18}\text{O}/^{16}\text{O}$ ratios in snow samples with $w(\text{NO}_3^-)$ as low as 10.0 ng g^{-1} , which can be analyzed
159 directly without a pre-concentration step (i.e. for a 5 nmol NO_3^- run, a sample of 10.0 ng g^{-1} requires a 31
160 mL injection).

161 NO_3^- isotopic ratios ($\delta^{15}\text{N}(\text{NO}_3^-)$, $\delta^{17}\text{O}(\text{NO}_3^-)$, $\delta^{18}\text{O}(\text{NO}_3^-)$) are defined as

162 $\delta = R_{\text{sample}}/R_{\text{standard}} - 1$ (Eq. 1),

163 where R is $^{15}\text{N}/^{14}\text{N}$, $^{17}\text{O}/^{16}\text{O}$, or $^{18}\text{O}/^{16}\text{O}$. $\delta^{15}\text{N}(\text{NO}_3^-)$ and $\delta^{18}\text{O}(\text{NO}_3^-)$ values are reported in per mil (‰)
164 relative to atmospheric N_2 ($\delta^{15}\text{N}_{\text{air}}=0\text{‰}$) and Vienna Standard Mean Ocean Water (VSMOW $\delta^{18}\text{O}=0\text{‰}$),
165 respectively. All of the isotopic data were calibrated using the international reference materials IAEA-NO-3,
166 USGS-35, USGS-34 and USGS-32 (Michalski et al., 2002; Böhlke et al., 2003). Determining the isotopic
167 composition in large volume samples has been extensively tested in the laboratory, and it is critical to run
168 reference materials very close to the same concentrations (i.e. same volume injections) as samples, to
169 eliminate any potential volume effects. Included in the supplementary materials are data from internal
170 working standards that show excellent reproducibility over a variety of injection volumes in different runs
171 (Tables S1 and S2). Precision of the isotopic analyses is calculated in two ways. First, the pooled standard
172 deviation ($1\sigma_p$) of all standards run within individual sample sets was calculated, as used in a previous study
173 (Buffen et al., 2014). For $\delta^{15}\text{N}(\text{NO}_3^-)$, the $1\sigma_p$ of standards is 0.3‰ (IAEA-NO-3, $n=80$), 0.3‰ (USGS-34,
174 $n=80$), 1.1‰ (USGS-32, $n=53$); and for $\delta^{18}\text{O}(\text{NO}_3^-)$ this is 0.6‰ (IAEA-NO-3, $n=80$), 0.6‰ (USGS-34,
175 $n=80$) and 0.7‰ (USGS-35, $n=80$). Second, the pooled standard deviation of all replicate samples run in at
176 least two different sets was examined ($n=38$ pairs of samples) and yielded 0.8‰ for $\delta^{15}\text{N}(\text{NO}_3^-)$ and 0.5‰
177 for $\delta^{18}\text{O}(\text{NO}_3^-)$. The pooled standard deviation of the replicate samples is probably the most representative
178 measure of precision as it accounts for the total variation within the denitrifier method (i.e., from sample
179 preparation to isotopic determination), and the variance is not diluted compared to the much higher number
180 of standards that are pooled across sample sets (compared to individual samples that are only run once or
181 twice).

182 During the NO_3^- reduction by bacteria, a small number of oxygen atoms may be exchanged between
183 water and the intermediates of denitrification (e.g., NO_2^-) and must be corrected for the isotopic
184 determination. In general, this exchange is $< 10 \%$, and typically $< 3\%$, of the total O atoms in the produced
185 N_2O and is corrected for using the measured oxygen isotope compositions of snow ($\delta^{18}\text{O}(\text{H}_2\text{O})$) and water
186 in the bacteria/media (see Casciotti et al., 2002; Kaiser et al., 2007 for correction schemes). $\delta^{18}\text{O}(\text{H}_2\text{O})$ was
187 determined using the standard CO_2 equilibration method (Johnsen et al., 1997). The standard deviation of
188 reference (VSMOW) measurements ($n=20$) was 0.10‰. Full snowpit profiles of $\delta^{18}\text{O}(\text{H}_2\text{O})$ were only
189 completed for P1 and P7, while only surface snow samples (3 cm) were measured for P2-P6.

190 A correction is also needed for $\delta^{15}\text{N}(\text{NO}_3^-)$ to account for the contribution of the $^{14}\text{N}^{14}\text{N}^{17}\text{O}$ isotopologue
191 to the m/z 45 signal measured by the IRMS (Kaiser et al., 2007). Because atmospheric NO_3^- contains a
192 non-zero $\Delta^{17}\text{O}$ (i.e., $\Delta^{17}\text{O} = \delta^{17}\text{O} - 0.52 \times \delta^{18}\text{O} > 0\text{‰}$), simply assuming $\delta^{17}\text{O} = 0.52 \times \delta^{18}\text{O}$ can yield an
193 overestimate of the true $\delta^{15}\text{N}(\text{NO}_3^-)$ by as much as 1-2‰ (Sigman et al., 2001; Hastings et al., 2003;
194 Savarino et al., 2007). To account for this contribution, a measured or estimated $\Delta^{17}\text{O}(\text{NO}_3^-)$ is used to

195 correct the $\delta^{15}\text{N}(\text{NO}_3^-)$ values. Previous East Antarctic investigations have shown that $\Delta^{17}\text{O}(\text{NO}_3^-)$ mainly
196 ranges from 25 to 35‰ in snow NO_3^- (Erbland et al., 2013) and we find a similar range for P1 in our study
197 (see below). For P1, the measured $\Delta^{17}\text{O}(\text{NO}_3^-)$ values reported below were used to correct $\delta^{15}\text{N}(\text{NO}_3^-)$, while
198 a mid-range value of $\Delta^{17}\text{O}(\text{NO}_3^-)=30\text{‰}$ was used for P2-P7. Using this mid-range value of $\Delta^{17}\text{O}(\text{NO}_3^-)=30\text{‰}$
199 leads to an average $\delta^{15}\text{N}(\text{NO}_3^-)$ difference of 1.6‰ compared to using $\Delta^{17}\text{O}(\text{NO}_3^-)=0\text{‰}$. A difference of +/-
200 5‰ in the $\Delta^{17}\text{O}(\text{NO}_3^-)$ used to correct the data (i.e., $\Delta^{17}\text{O}(\text{NO}_3^-)=25\text{‰}$ or 35‰) results in a $\delta^{15}\text{N}(\text{NO}_3^-)$
201 difference of 0.3‰, which is comparable to our reported analytical precision and is negligible when
202 compared to the range of sample $\delta^{15}\text{N}(\text{NO}_3^-)$ values.

203 For determination of $\Delta^{17}\text{O}(\text{NO}_3^-)$, the sample N_2O produced by the denitrifier method was thermally
204 decomposed to N_2 and O_2 in a heated gold tube, and the O_2 was then measured at m/z 32 and 33 signals on
205 the IRMS (Kaiser et al., 2007). A minimum of 35 nmol NO_3^- is needed for the analysis, but the low $w(\text{NO}_3^-)$
206 and low sample volumes available in this study limited the measurement of both $\Delta^{17}\text{O}(\text{NO}_3^-)$ and $\delta^{15}\text{N}$ and
207 $\delta^{18}\text{O}$ on the same sample. A pre-concentration procedure is needed for the measurement of $\Delta^{17}\text{O}(\text{NO}_3^-)$ (e.g.,
208 Morin et al., 2008; Frey et al., 2009; Erbland et al., 2013). Briefly, NO_3^- was trapped in an anion exchange
209 resin, and then eluted by a 1M NaCl solution. A variety of NaCl salts were tested and found to contain NO_3^- ,
210 and thus procedural blanks were determined for each batch of NaCl used. (Note that NO_3^- was found in
211 every batch of NaCl (Fisher Scientific) tested, ranged from 478 to 547 ng g⁻¹, and was different even for
212 bottles with the same lot number.) For the samples from P1, 28ng g⁻¹ was measured for the 1M solution of
213 NaCl used for elution. During the concentrating procedure, one Milli-Q water blank and two sets of
214 standards (USGS-34 and USGS-35) with similar $w(\text{NO}_3^-)$ to the snow samples were processed
215 simultaneously. The measured $\Delta^{17}\text{O}(\text{NO}_3^-)$ was then corrected by two steps: (1) $\Delta^{17}\text{O}(\text{NO}_3^-)$ in concentrated
216 samples was linearly corrected using the standards USGS-34 and USGS-35 run within individual sample
217 sets; and (2) the output of step (1) was further corrected by the standards used during the concentration
218 procedure to account for the impact of procedural influence (e.g., the NaCl blank). A mean difference of 2.5‰
219 for $\Delta^{17}\text{O}(\text{NO}_3^-)$ was obtained without the step (2) correction. Precision for repeated measurement of
220 $\Delta^{17}\text{O}(\text{NO}_3^-)$ is only 0.44‰ (see also Table S2), but without correcting for the blank associated with the
221 eluent NaCl, we find that the pre-concentration method can result in an underestimation at least on the order
222 of 2.5‰ for $\Delta^{17}\text{O}(\text{NO}_3^-)$.

223

224 **3 Results**

225

226 **3.1 Snowpit $w(\text{NO}_3^-)$**

227

228 A summary for all measurements of $w(\text{NO}_3^-)$, $\delta^{15}\text{N}(\text{NO}_3^-)$ and $\delta^{18}\text{O}(\text{NO}_3^-)$ in each snowpit is given in Fig.
229 2 and the detailed profiles with depth are illustrated in Fig. 3. In general, $w(\text{NO}_3^-)$ is lower than 200 ng g⁻¹ in
230 P1 and P2, which are characterized with higher annual snow accumulation (see Fig. 1), and large,
231 quasi-regular fluctuations of $w(\text{NO}_3^-)$ are present in both pits. In contrast, pits P4-P7 from the lower snow
232 accumulation sites show the highest $w(\text{NO}_3^-)$ in surface snow, which falls sharply from >200 ng g⁻¹ near the
233 surface to below 50 ng g⁻¹ within the top meter, and do not contain regular fluctuations. The markedly
234 decreasing trend of $w(\text{NO}_3^-)$ with depth seems to fit an exponential model as has been done previously
235 (Traversi et al., 2009).

236

237 **3.2 Isotopic compositions of NO_3^-**

238

239 For $\delta^{15}\text{N}(\text{NO}_3^-)$ and $\delta^{18}\text{O}(\text{NO}_3^-)$, the coastal and inland pits differ greatly in terms of the average values
240 and the variability with depth. For the coastal sites P1-P3, $\delta^{15}\text{N}(\text{NO}_3^-)$ is generally lower than in the inland
241 snowpits P4-P7, varying between -14.8 and 70.8‰, while $\delta^{15}\text{N}(\text{NO}_3^-)$ in the inland pits ranges from 15.5 to
242 460.8‰ (Figs. 2 and 3). This high value of 460.8‰ in pit P7 (which is at Dome A) is the highest natural
243 $\delta^{15}\text{N}(\text{NO}_3^-)$ on Earth so far reported to our knowledge. In the inland pits (P4-P7), $\delta^{15}\text{N}(\text{NO}_3^-)$ is lower in the
244 uppermost layers and strongly increases deeper in the snowpack, with most of the increase occurring in the
245 top 20-30 cm.

246 In contrast to $\delta^{15}\text{N}(\text{NO}_3^-)$, $\delta^{18}\text{O}(\text{NO}_3^-)$ is higher on average in the coastal pits (P1-P3), ranging between
247 52.5 and 111.2 ‰, compared to the inland sites (P4-P7) where $\delta^{18}\text{O}(\text{NO}_3^-)$ varies between 16.8 and 84.0 ‰
248 (Figs. 2 and 3). It is noted that the averages of $\delta^{18}\text{O}(\text{NO}_3^-)$ for P4-P7 are comparable, while $\delta^{15}\text{N}(\text{NO}_3^-)$
249 means vary significantly, from 133.6 to 335.2‰. There is no obvious trend in the $\delta^{18}\text{O}(\text{NO}_3^-)$ profiles with
250 depth in P1-P3, but this is not the case for the inland sites. $\delta^{18}\text{O}(\text{NO}_3^-)$ decreases over the top 20-30 cm, but
251 gradual and consistent increases are observed below 30 cm in P4, P5 and P7 which continue to the pit base
252 (200-300 cm; Fig. 3). A similar decrease in $\delta^{18}\text{O}(\text{NO}_3^-)$ is observed in the top of P6, but it is not clear if an
253 increasing trend exists in the profile below.

254 $\Delta^{17}\text{O}(\text{NO}_3^-)$ of P1 varies from 25.2 to 42.9‰, with an average of 32.8‰ (Fig. 2). In general, the variation
255 trend of $\Delta^{17}\text{O}(\text{NO}_3^-)$ is similar to that of $\delta^{18}\text{O}(\text{NO}_3^-)$ (Fig. 7), and a close relationship was observed between
256 the two ($r^2=0.77$, $p<0.001$).

257 The difference between the coastal and inland pits observed here is similar to that observed in the Erbland
258 et al. (2013) study. A comparison between the two studies is presented in the supplementary materials as Fig.
259 S1.

260

261 4 Discussion

262

263 After deposition, NO_3^- can be lost from snow by photolysis and volatilization as HNO_3 (sometimes
264 referred to as evaporation or physical release in other studies), and the extent of loss via these
265 post-depositional processes is expected to be accumulation dependent (Röthlisberger et al., 2002; Grannas et
266 al., 2007). At lower accumulation sites, NO_3^- loss is relatively high, synchronous with a large degree of
267 isotopic fractionation (Blunier et al., 2005; Frey et al., 2009; Erbland et al., 2013). In contrast,
268 post-depositional alteration of snow NO_3^- in high accumulation regions can be minor, and seasonal and
269 interannual cycles can be preserved in the snowpack (e.g., Wagenbach et al., 1994; Hastings et al., 2004).

270 Based on the site differences in annual snow accumulation rate and the profile trends of $w(\text{NO}_3^-)$,
271 $\delta^{15}\text{N}(\text{NO}_3^-)$ and $\delta^{18}\text{O}(\text{NO}_3^-)$, the seven pits are divided into two groups within the following discussion:
272 group I includes the coastal, medium-high accumulation sites P1-P3 ($>91 \text{ kg m}^{-2} \text{ a}^{-1}$) and group II are the
273 low accumulation and further inland sites P4-P7 ($<55 \text{ kg m}^{-2} \text{ a}^{-1}$). Below we consider what processes (and
274 fractionation constants) can explain observations from the group I and group II snowpits, and whether it is
275 possible to predict values at depth based on the loss processes near the surface.

276

277 4.1 NO_3^- loss in inland upper snowpack

278

279 If it is assumed that post-depositional loss of snow NO_3^- is accompanied by a Rayleigh-type fractionation,
280 the observed changes in $\delta^{15}\text{N}$ and $\delta^{18}\text{O}$ in a snowpit profile can be described as a function of $w(\text{NO}_3^-)$ via

281
$$\ln(\delta_{\text{snow}}+1) = \varepsilon * \ln(w_{\text{snow}}) + [\ln(\delta_{\text{snow},0}+1) - \varepsilon * \ln(w_{\text{snow},0})] \text{ (Eq. 2),}$$

282 where $\delta_{\text{snow},0}$ and δ_{snow} denote isotopic ratios in the initial and remaining NO_3^- , respectively, and $w_{\text{snow},0}$ and

283 w_{snow} are the initial and remaining NO_3^- mass fractions, respectively (e.g., Blunier et al., 2005). ϵ can be
 284 obtained from the slope of the linear regression for $\ln(w_{\text{snow}})$ vs. $\ln(\delta_{\text{snow}}+1)$, while $[\ln(\delta_{\text{snow},0}+1) -$
 285 $\epsilon \cdot \ln(w_{\text{snow},0})]$ would be the intercept. It is noted that ϵ is related to the fractionation factor α by $\epsilon = \alpha - 1$ (Criss,
 286 1999).

287 Solar radiation decreases exponentially in the snowpack, with attenuation described in terms of an
 288 e -folding depth (z_e) where the actinic flux is reduced to $1/e$ (37%) of the surface value. Accordingly, roughly
 289 95% of snowpack photochemistry should occur above the depth of three times z_e (Warren et al., 2006). For
 290 the individual pits here, we calculate apparent ϵ values (ϵ_{app}) from data in the upper 20cm, 40cm and 60cm,
 291 to evaluate the impacts of post-depositional processes on snow NO_3^- (Table 2). Zatko et al. (2013)
 292 calculated a z_e of about 20cm for remote Antarctic sites. For group II, relatively strong relationships are
 293 observed between $w(\text{NO}_3^-)$ and $\delta^{15}\text{N}(\text{NO}_3^-)$ or $\delta^{18}\text{O}(\text{NO}_3^-)$ in the top 60 cm (as indicated by the statistically
 294 significant r^2 values for Eq. 2; Table 2). These pits are characterized by negative $^{15}\epsilon_{\text{app}}$, with values of -77.8‰
 295 (P4), -93.1‰ (P5), -50.2‰ (P6) and -61.3‰ (P7) for the upper 20cm snow layer (i.e., the 0-20cm interval;
 296 Table 2); whereas $^{18}\epsilon_{\text{app}}$ values are positive, indicating a depletion of $^{18}\text{O}(\text{NO}_3^-)$ with decreasing $w(\text{NO}_3^-)$.
 297 The observed fractionation constants ($^{15}\epsilon_{\text{app}}$ and $^{18}\epsilon_{\text{app}}$) for group II (P4-P7) are comparable to those from
 298 other snowpits on the East Antarctic plateau (Frey et al., 2009; Erbland et al., 2013; see also Fig. S1).

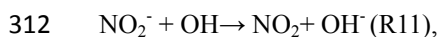
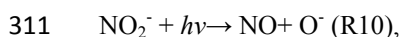
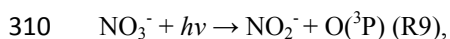
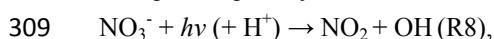
299 In the upper 20 cm of the snowpack, a significant NO_3^- loss with increasing depth is seen in the group II
 300 pits and corresponds to a large enrichment of $^{15}\text{N}(\text{NO}_3^-)$. A large loss of NO_3^- leading to such high
 301 $\delta^{15}\text{N}(\text{NO}_3^-)$ values in the surface snow is consistent with the calculated low $^{15}\epsilon_{\text{app}}$ in the upper snowpack and
 302 our expectations based on other findings in East Antarctica (e.g., Savarino et al., 2007; Erbland et al., 2013).
 303 Such strongly positive $\delta^{15}\text{N}$ values (>100‰) have not been observed in atmospheric NO_3^- .

304

305 4.1.1 Photolytic loss of NO_3^-

306

307 Photolysis of snow NO_3^- is thought to primarily occur within a disorder interface, sometimes referred to
 308 as a quasi-liquid layer, at the surface of the ice crystal via the reactions



313 with R8 exceeding R9 by a factor of 8-9 (Warneck and Wurzinger, 1988; Dubowski et al., 2001; Chu and
 314 Anastasio, 2003). Snow NO_3^- photolysis products are mainly NO_2 , greatly exceeding NO under most
 315 conditions (Dibb et al., 2002). Under acidic conditions ($\text{pH} < 5$), $\text{HONO}_{(\text{g})}$ formation from NO_2^- protonation
 316 is also important (Grannas et al., 2007 and references therein). Only NO_2 produced near the ice surface-air
 317 interface can be released to the firm air and subsequently escape from the snowpack to the overlying
 318 atmosphere (Boxe et al., 2005).

319 In order to identify the relative importance of photolysis and volatilization (section 4.1.3) on NO_3^- loss,
 320 the fractionation constant of each process should first be quantified. The photolysis rate constant $j_{\text{NO}_3^-}$ (s^{-1}) is
 321 expressed as

322
$$j_{\text{NO}_3^-} = \int \sigma_{\text{NO}_3^-}(\lambda, T) \times \phi_{\text{NO}_3^-}(\lambda, T, \text{pH}) \times I(\lambda) d\lambda$$
 (Eq. 3),

323 where $\sigma_{\text{NO}_3^-}$ (cm^2) is the spectral absorption cross section (Chu and Anastasio, 2003); $\phi_{\text{NO}_3^-}$ is the quantum
 324 yield (0-1), which was calculated to be 1.7×10^{-3} at 239K and $\text{pH} = 5$ (Chu and Anastasio, 2003), and I is the

325 spectral actinic flux (photons $\text{cm}^{-2} \text{sec}^{-1} \text{nm}^{-1}$). Frey et al. (2009) proposed a theoretical model for estimating
326 nitrate photolytic isotopic fractionation constants, which is based on a framework originally developed by
327 Yung and Miller (1997) for stratospheric N_2O . The framework exploits mass-dependent differences in the
328 vibrational frequencies and ground-state energies for a given set of isotopologues. These differences result
329 in a modeled spectral absorption cross section for the heavier isotopologue which is shifted to longer
330 wavelengths, thus influencing the rate constant. The isotopic fractionation constant can then be calculated
331 by

$$332 \quad \varepsilon = (j/j') - 1 \text{ (Eq. 4),}$$

333 where j corresponds to the heavy isotopologue (e.g., $^{15}\text{N}^{16}\text{O}_3^-$), and j' corresponds to the light isotopologue
334 (e.g., $^{14}\text{N}^{16}\text{O}_3^-$), and it is assumed that the different isotopologues retain similar spectral absorption curves
335 and equal quantum yields.

336 We calculate the photolytic $^{15}\varepsilon$ and $^{18}\varepsilon$ at sites P1 and P7 for peak summer radiation conditions (solstice
337 solar noon on December 21, 2012) using actinic fluxes derived from the Tropospheric Ultraviolet and
338 Visible (TUV5.0) radiation transfer model (Madronich and Flocke, 1998) assuming clear sky conditions and
339 a total overhead ozone column of 300 DU for both sites. We use the nitrate absorption cross section from
340 Chu and Anastasio (2003) and calculate quantum yields using the equation given in this same work for
341 -10°C at P1 and -30°C at P7.

342 The resulting fractionation constants are $^{15}\varepsilon = -45.3\text{‰}$ (P1) and -48.0‰ (P7) and $^{18}\varepsilon = -32.5\text{‰}$ (P1) to
343 -34.4‰ (P7), and the relatively small variability between the two sites indicates that the calculated values
344 are representative for the two site groupings. Berhanu et al. (2014) have recently proposed absorption cross
345 sections derived from the measurements of Chu and Anastasio (2003) but modeled directly for the $^{14}\text{N}^{16}\text{O}_3^-$
346 and $^{15}\text{N}^{16}\text{O}_3^-$ isotopologues at -30°C . When using these cross sections, $^{15}\varepsilon$ is calculated to be -48.9‰ at P1
347 and -52.8‰ at P7.

348 The negative ε values suggest that photolysis will lead to a strong enrichment of both ^{15}N and ^{18}O in NO_3^-
349 remaining in the snow. For $^{15}\varepsilon_{app}$ calculated from observations in the upper 60 cm of the group II pits (Table
350 2), the higher r^2 values imply that photolysis can largely explain enrichment of ^{15}N with the decrease of
351 $w(\text{NO}_3^-)$. At Dome C, where snow accumulation is typically less than $50 \text{ kg m}^{-2} \text{ a}^{-1}$, close to the values of
352 P4-P7 (Fig. 1), photolysis has also been reported as responsible for large increases in $\delta^{15}\text{N}(\text{NO}_3^-)$ with depth
353 in the snow (Frey et al., 2009; Erbland et al., 2013). The negative calculated $^{18}\varepsilon$, however, does not agree
354 with the highly positive $^{18}\varepsilon_{app}$ values based on the observations.

355

356 4.1.2 Aqueous phase “secondary” NO_3^- formation

357

358 If the post-depositional loss of NO_3^- in the group II pits was driven solely by photolysis, ^{18}O should also
359 be enriched in the remaining NO_3^- according to the modeled photolytic $^{18}\varepsilon$ values (-32.5 to -34.4‰).
360 However, $\delta^{18}\text{O}$ decreases over the top 20 cm (Fig. 3) and the apparent $^{18}\varepsilon$ values ($^{18}\varepsilon_{app}$) calculated from the
361 observed data in the upper 20cm are instead positive, varying from 16.7 to 30.2‰ (Table 2). Furthermore,
362 simple photolysis will lead to a linear relationship of $\delta^{18}\text{O}(\text{NO}_3^-)$ vs. $\delta^{15}\text{N}(\text{NO}_3^-)$ with a slope of roughly 0.7,
363 i.e., equal to the ratio of the fractionation constants. However, there are negative relationships between
364 $\delta^{18}\text{O}(\text{NO}_3^-)$ and $\delta^{15}\text{N}(\text{NO}_3^-)$ in the top 20 cm (Fig. 4), with slopes varying from -0.4 to -0.2 .

365 Similar negative relationships have been observed in other East Antarctic snowpits (Frey et al., 2009;
366 Erbland et al., 2013) and, following from experimental and theoretical work (McCabe et al., 2005; Jacobi
367 and Hilker, 2007), were attributed to the aqueous-phase re-oxidation of the products of NO_3^- photolysis (e.g.,
368 NO_2) by OH and/or H_2O to form “secondary” NO_3^- .

369 In this way, the O atoms from OH/H₂O provide a depleted ¹⁸O source while δ¹⁵N(NO₃⁻) is seemingly not
 370 affected. For the group II pits, δ¹⁸O(H₂O) in surface snow falls roughly in the range of -45 to -60‰. These
 371 effects can explain the observed positive ¹⁸ε_{app} values and negative relationships between δ¹⁸O(NO₃⁻) and
 372 δ¹⁵N(NO₃⁻) in the top 20 cm. (Direct exchange of O atoms between NO₃⁻ and H₂O is only thought to be
 373 important at NO₃⁻ concentrations that are orders of magnitude higher than those found in snow (Bunton et
 374 al., 1952)).

375 For the top 2.5 cm of snow in P7, w(NO₃⁻) and δ¹⁸O(NO₃⁻) is 374 ng g⁻¹ and 74.9‰ respectively, while
 376 w(NO₃⁻) decreases to 37.6 ng g⁻¹ at a depth of 20cm. Based on the modeled effect of photolysis, δ¹⁸O in the
 377 remaining NO₃⁻ at 20 cm could be predicted by

$$378 \delta^{18}\text{O}_{\text{remaining}} = (1 + \delta^{18}\text{O}_0) * f^{(1/\epsilon)} - 1 \text{ (Eq. 5),}$$

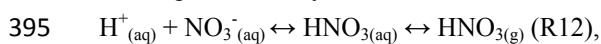
379 where δ¹⁸O_{remaining} represents δ¹⁸O in the remaining NO₃⁻; δ¹⁸O₀ is that of initial NO₃⁻; *f* is the fraction of
 380 NO₃⁻ remaining in the snow; and ¹⁸ε is the photolysis fractionation constant (-34.4‰). If photolysis alone is
 381 responsible for the NO₃⁻ loss, δ¹⁸O(NO₃⁻) is expected to be 161‰ at 20cm and thus the observed δ¹⁸O of
 382 42.6‰ requires a cumulative 54% exchange of O atoms in the remaining NO₃⁻ assuming a δ¹⁸O(H₂O) of
 383 -60‰. For P4, P5 and P6, this exchange is estimated to be 48%, 40% and 11%, respectively. (It is noted that
 384 the exchange percent in P6 is relatively small, associated with the small difference in mass fractions and
 385 δ¹⁸O of NO₃⁻ between the surface snow sample (w(NO₃⁻)=203 ng g⁻¹, δ¹⁸O(NO₃⁻)=70‰) and the snow at a
 386 depth of 20cm (w(NO₃⁻)=125 ng g⁻¹, δ¹⁸O(NO₃⁻)=72‰). This simple mass balance approach, overall,
 387 indicates that re-oxidation plays a very significant role in determining how the δ¹⁸O of NO₃⁻ evolves in the
 388 snow column during burial.

389

390 4.1.3 Volatile loss of NO₃⁻

391

392 Volatilization, or physical release, of HNO₃ may also be a pathway for post-depositional loss of NO₃⁻ in
 393 snow (Röthlisberger et al., 2000; Erbland et al., 2013). The importance of this process is unclear, however,
 394 as loss proceeds only as HNO₃,



396 and thus requires highly acidic conditions given the very high dissociation constant for HNO₃ (Sato et al.,
 397 2008). Volatilization may also be inhibited at low temperatures as suggested by laboratory and field
 398 observations (Erbland et al., 2013; Berhanu et al., 2014).

399 The current understanding of the isotopic impact of volatilization is somewhat limited. An experiment
 400 conducted by Erbland et al. (2013) at Dome C suggested that the ¹⁵ε (mean±1σ) for volatilization varied
 401 from 0.9±3.5‰ (-30 °C) to -3.6±1.1‰ (-10 °C) (i.e., close to non-fractionating). However, the loss of nitrate
 402 in these experiments may have been driven by the large losses of snow via sublimation. No observational or
 403 experimental data for ¹⁸ε are available. Theoretical model estimates of volatile fractionation, assuming that
 404 the aqueous-phase equilibrium in R12 is the controlling step in the overall fractionation (Frey et al., 2009),
 405 predict values of ¹⁵ε and ¹⁸ε to be from 12.6‰ (0 °C) to 16.8‰ (-73 °C) and between 1.1‰ (0 °C) and 0.6‰
 406 (-73 °C), respectively (Table S3).

407 For the summertime temperatures at the P4-P7 sites (<-30 °C), physical release should deplete both ¹⁵N
 408 and ¹⁸O in the remaining snow NO₃⁻ according to the modeled ε values, whereas the field experiment
 409 observations would suggest negligible change in δ¹⁵N with decreasing w(NO₃⁻) in the snow. The
 410 observations for P4-P7 show increasing δ¹⁵N(NO₃⁻) with decreasing w(NO₃⁻), and that δ¹⁵N(NO₃⁻) is
 411 negatively correlated with δ¹⁸O(NO₃⁻) (Fig. 4), disagreeing with both expectations (i.e., field experiment
 412 observations and modeled results; Table S3). The current understanding of volatile fractionation, however,

413 is very limited and experimental data for $^{18}\epsilon$ are not available to date. Nevertheless, little evidence is found
414 to support a significant influence of volatilization at our sites given the existing state of knowledge.

415

416 **4.2 Isotopic variability with depth at inland sites (group II snowpits)**

417

418 As shown in Table 2, the logarithmic relationships between $\delta^{15}\text{N}$ or $\delta^{18}\text{O}$ and mass fraction of NO_3^- are
419 strongest in the upper 60 cm, as seen in the r^2 values. While generally weaker in the layers below, the r^2
420 values remain significant even when the entire snowpit is considered. For instance, for $^{15}\epsilon_{app}$, P4, P5, and P6
421 all have r^2 above 0.5 (with a $p < 0.05$) when observations from the entire snowpit are considered.
422 Interestingly, while $\delta^{15}\text{N}(\text{NO}_3^-)$ maintains a negative relationship with $w(\text{NO}_3^-)$ at all depths, the
423 relationships between $\delta^{18}\text{O}(\text{NO}_3^-)$ and $w(\text{NO}_3^-)$ shift from being positive in the upper 20 cm to generally
424 negative in the deeper snow (Table 2; Fig. 5). This leads to there generally being no association between
425 $w(\text{NO}_3^-)$ and $\delta^{18}\text{O}(\text{NO}_3^-)$ when the entire snowpit depth interval is considered (Table 2).

426 It is also useful to discuss this variability with depth in terms of the isotopic fractionation constants. If
427 there was only a single isotopically fractionating process driving the observed changes in the snow, such as
428 photolysis, the apparent fractionation constants for $\delta^{15}\text{N}(\text{NO}_3^-)$ and $\delta^{18}\text{O}(\text{NO}_3^-)$ would be similar throughout
429 the snow column. This expectation relies on two important assumptions. First, the boundary conditions that
430 influence the fractionation constants remain similar over time. This is to say that factors such as the
431 contribution of different NO_3^- sources, accumulation rate, the influence of total overhead ozone on the
432 spectral actinic flux and photolysis rate, and the influence of snow chemistry on photolability of NO_3^- (e.g.,
433 Davis et al., 2008; Meusinger et al., 2014), remain similar over time. Second, the isotopic imprint of
434 photolysis is set in the upper snowpack and then preserved below. This requires the assumption that once
435 NO_3^- is moved below the photic zone, no additional in situ modifications take place. Stemming from these
436 expectations, the isotopic composition of buried NO_3^- could be back-calculated to that originally at the
437 surface if the isotopic imprint of alteration at the surface could be quantified in terms of a fractionation
438 constant.

439 Based on the observations with depth, it is clear that the ϵ_{app} values are dependent on the depth range
440 chosen (Table 2). Both $^{15}\epsilon_{app}$ and $^{18}\epsilon_{app}$ vary but with distinct differences. The $^{15}\epsilon_{app}$ tends to become more
441 positive with depth, while $^{18}\epsilon_{app}$ decreases and even switches from positive to negative values. When taken
442 together with variability in the strength of the isotopic relationships with $w(\text{NO}_3^-)$ and the observation that
443 isotopic composition continues to change below the expected photic zone depths, especially for $\delta^{18}\text{O}(\text{NO}_3^-)$
444 (Fig. 3), it would seem that the assumptions above do not all apply. Either the fractionation constants change
445 over time because of a change in boundary conditions and/or the isotopic imprint of photolysis is not
446 preserved below the photic zone. The former hypothesis is much more likely as, thus far, there is little other
447 evidence of processes well below the photic zone modifying buried NO_3^- .

448

449 **4.3 Predicting $w(\text{NO}_3^-)$, $\delta^{15}\text{N}(\text{NO}_3^-)$ and $\delta^{18}\text{O}(\text{NO}_3^-)$ values in buried snow**

450

451 Erbland et al. (2013) proposed that snow $w(\text{NO}_3^-)$ and isotopic compositions may approach constant
452 values, called “asymptotic” values, below the photic zone (or zone of active NO_3^- loss). By means of an
453 exponential decrease regression, asymptotic values are calculated by

$$454 M(x) = M_{(as.)} + [M_{(0)} - M_{(as.)}] \times \exp(-c \times x) \text{ (Eq. 6),}$$

455 where $M_{(x)}$ is the $w(\text{NO}_3^-)$, $\delta^{15}\text{N}(\text{NO}_3^-)$ or $\delta^{18}\text{O}(\text{NO}_3^-)$ at depth x (cm); $M_{(as.)}$ is the asymptotic value for these
456 parameters; $M_{(0)}$ is the value at the surface of the snowpit; and c is a constant. Asymptotic values for each

457 snowpits are calculated from the best fit (minimizing the sum of squared residuals) of $M_{(x)}$ vs. depth.

458 Based on observations from only the top 20 cm of snow in different snowpits on the EAIS, the Erbland et
459 al. (2013) study predicted values below the photic zone based upon an exponential decrease regression.
460 Because our snowpits extend deeper along the entire traverse, and as seen in Fig. 3 the snowpits did not
461 typically follow a simple exponential decrease, we explored whether the asymptotic values change when
462 derived from different depth ranges in the snowpit. In order to compare the asymptotic values derived from
463 different snow depth ranges, observations from four intervals (0-20cm, 0-40cm, 0-60cm, and 0-100cm)
464 were selected to make this calculation and the results are listed in Table 3. Several interesting results emerge.
465 For asymptotic calculations of $w(\text{NO}_3^-)$, $\delta^{15}\text{N}(\text{NO}_3^-)$ and $\delta^{18}\text{O}(\text{NO}_3^-)$, all show important variations
466 depending on the depth interval over which they are calculated. The variance, described in Table 3 by the
467 standard error, is relatively large for the asymptotic values, but generally decreases the more observations
468 that are included. In concert with this, the greater amount of observations included in the calculation the
469 better the fit of the predicted values with the observed values as evidenced by the changing r^2 with
470 calculations over different depth intervals. The sensitivity of the calculation of asymptotic values for
471 different depth intervals in each of the group II snowpits is shown in Fig. 6.

472 What is the depth interval over which it is necessary to calibrate the asymptotic calculation? In other
473 words, how much information must we know about surface conditions to make the asymptotic relationship
474 useful for predicting isotope values at depth? Fig. 6 clearly shows that the more observations that are
475 included the better the fit to the data will be, which is logical. But the range of profiles predicted by the
476 asymptotic regressions also make it clear that much more information exists in the observations than can be
477 explained by the simple assumption that photolytic loss, particularly in the top 20cm, is the overwhelming
478 signal captured at this low accumulation sites. Overall, the $\delta^{18}\text{O}(\text{NO}_3^-)$ in deeper snow is more difficult to
479 predict compared to $w(\text{NO}_3^-)$ and $\delta^{15}\text{N}(\text{NO}_3^-)$. This conclusion is consistent with the changes in $\delta^{18}\text{O}$ at
480 deeper depths (Fig. 3) and the changes in ϵ_{app} with depth (Table 2).

481 In cases where there is significant post-depositional loss and/or processing of NO_3^- , the $\delta_{(as.)}$, in theory,
482 could help account for the impact of post-depositional processing compared to preservation in
483 reconstructing a primary atmospheric signal. Our results show that $\delta_{(as.)}$ (and ϵ_{app}) is sensitive to the depth
484 interval over which exponential decrease is assumed. As suggested above, changes in factors such as the
485 contribution of different NO_3^- sources, accumulation rate, total overhead ozone, and the influence of snow
486 chemistry on photolability of NO_3^- may not remain similar over the time period covered by the snowpits.
487 There do not appear to be significant trends in the annual accumulation rates based on data from Dome A.
488 Wang et al. (2013) have compiled existing stake and snowpit accumulation measurements from Dome A and
489 show 1) little spatial variability (surrounding 50 km) and 2) stable accumulation rates over recent decades
490 and since 1260 AD (1965-2009 = 21 kg m⁻² a⁻¹; 2005-2008 = 18 kg m⁻² a⁻¹; 2005-2009 = 19 kg m⁻² a⁻¹;
491 2008-2009 = 21 kg m⁻² a⁻¹; and 1260-2005 = 21.6 to 23 kg m⁻² a⁻¹). Automatic weather station
492 measurements presented in the same work show somewhat higher accumulation in the spring and summer
493 (roughly 6-7 mm per month) vs. fall and winter (roughly 3-6 mm per month) with fairly stable values in the
494 warmer months. Based on the Dome A studies, it is unlikely that significant changes in accumulation have
495 occurred in the area of the group II snowpits. Therefore, this cannot explain the difference between what is
496 predicted based upon the $\delta_{(as.)}$ and what is observed (Fig. 6). Nor does it seem likely that changes in ϵ_{app} can
497 be explained by accumulation rate. If it is assumed that snow accumulation has been constant for the group
498 II snowpits, then the snowpits can be roughly dated based on measured accumulation and snow density (Fig.
499 S2). This approximate dating suggests that the bottom of the P4 snowpit is about the year 2000; P5 dates
500 from ~1994; P6 from 1985; and P7 from 1970. All four snowpits show a change in the relationship between

501 $\delta^{18}\text{O}(\text{NO}_3^-)$ with $w(\text{NO}_3^-)$ and with $\delta^{15}\text{N}(\text{NO}_3^-)$ between near surface snow (<20 cm) and deeper snow (Fig.
502 5). Based on the approximate dating, the timing of this change is very different in the different snowpits. For
503 example, for a depth of 100 cm, snow in P4 is dated to ~2007, P5 to ~2004, and P6 and P7 to ~2000. (Even
504 given the imprecision of the dating method it is unlikely that more accurate dating would conclude that
505 changes in the snowpits occur exactly together.)

506 Can changes in stratospheric ozone concentration help to explain this change? Both the photolytic rate
507 constant and fractionation constants would be sensitive to significant changes in overhead ozone
508 concentration (i.e., less stratospheric ozone leads to more penetration of light at wavelengths that can
509 photolyze nitrate). Based on the approximate dating of the pits, P7 overlaps with the pre-ozone hole era
510 (generally considered prior to 1980), but there is no obvious change in the isotope observations (1980
511 occurs at a depth of about 250 cm; Fig. 3 and Fig. S2). Moreover, both ground-based observations at South
512 Pole and satellite-based observations (TOMS/OMI) do not show any significant trend in total overhead
513 ozone during spring and early summer over the time period 2000-2010
514 (<http://www.antarctica.ac.uk/met/jds/ozone/graphs.html>; http://www.cpc.noaa.gov/products/stratosphere/winter_bulletins/sh_09/http://ozonewatch.gsfc.nasa.gov/statistics/annual_data.html). This does not prove that
515 there is not a link between the observed changes in the isotopic composition of snow nitrate and overhead
516 ozone concentration, but this link over time is not obvious in this region. Finally, it is notable that the DC07
517 and DC04 pits (about 70 cm) from Frey et al. (2009) cover 8-10 years and thus overlap some with data from
518 P4-P7. Neither of the DC pits show increasing $\delta^{18}\text{O}(\text{NO}_3^-)$ with depth (or decreasing $\delta^{15}\text{N}(\text{NO}_3^-)$ such as that
519 in P7). Given the large spatial influence of stratospheric ozone on surface irradiance in Antarctica, it seems
520 unlikely that Dome A and its surrounding region would be affected by this process and not Dome C. This
521 suggests that something more localized, such as a change in the photolability of nitrate due to changes in
522 snow chemistry, may have an important influence in recent decades.

524

525 **4.4 Seasonal shifts in NO_3^- sources to coastal snow (group I snowpits)**

526

527 Pit profiles from the higher accumulation sites (group I) do not fit an exponential decrease function but
528 instead show periodic variability in mass fraction and isotopic composition of NO_3^- (Fig. 3),

529 As discussed above, sharp decreases in $w(\text{NO}_3^-)$ in the top few centimeters of inland East Antarctic
530 snowpits are interpreted as evidence of severe photolytic NO_3^- loss. $w(\text{NO}_3^-)$ in the top 10 cm of the coastal
531 P1 snowpit also decreases from the surface (Fig. 3) and, if viewed in isolation, could also be taken as
532 evidence for post-depositional loss. However, annual average snow accumulation at P1 is approximately 50
533 cm snow a^{-1} , and the full profile clearly shows that similarly high $w(\text{NO}_3^-)$ values are observed below 10 cm,
534 as would be expected from seasonal cycles. We expect that if the coastal sites studied by Erbland et al.
535 (2013) had been continuously sampled below 20 cm, similar features would have been observed. This
536 should serve as caution in interpreting the behavior of NO_3^- at high accumulation sites based on observations
537 that do not cover a full annual cycle of snowfall.

538 Profiles of the group I pits (P1-P3) show large variations in $w(\text{NO}_3^-)$ and isotopic composition throughout
539 the snowpack, with some correspondence to $\delta^{18}\text{O}(\text{H}_2\text{O})$ which is a proxy for temperature (Fig.7). The
540 seasonality is most apparent at site P1 due to the highest sampling resolution (3.0 cm per sample compared
541 to 5.0 cm per sample for pits P2 and P3) and highest snow accumulation rate (172 $\text{kg m}^{-2} \text{a}^{-1}$), though all
542 group I sites feature high accumulation rates above 91 $\text{kg m}^{-2} \text{a}^{-1}$ (Table 1).

543 It is difficult to assign samples to four distinct seasons based on $\delta^{18}\text{O}(\text{H}_2\text{O})$ alone, so we choose a
544 conservative classification of two periods: a warm season corresponding to higher $\delta^{18}\text{O}(\text{H}_2\text{O})$ and a cold

545 season characterized by lower $\delta^{18}\text{O}(\text{H}_2\text{O})$ (Fig. 7). These assignments are also consistent with other
546 established seasonal tracers measured in P1 in that the $\delta^{18}\text{O}(\text{H}_2\text{O})$ peaks (warm season) correspond to spikes
547 in MSA and low Na^+ , while the opposite pattern is present during the identified cold seasons (C-J. Li,
548 personal communication, 2014). The snow accumulation rate of $172 \text{ kg m}^{-2} \text{ a}^{-1}$ at P1 site, which corresponds
549 to 43-57 cm snow a^{-1} assuming a typical snow density of $0.3\text{-}0.4 \text{ g cm}^{-3}$, also fits with the thickness of the
550 designated seasonal layers. Although coarse, this conservative dating of the snowpit is sufficient to make
551 broad comparisons throughout the year. This is aided by the high accumulation rate and the large amplitude
552 variability in the data.

553 The samples and data assigned to warm and cold seasons for P1 are shown in Figs. 7 and 8. If the
554 $\delta^{18}\text{O}(\text{H}_2\text{O})$ peaks are taken to roughly correspond with the middle of the warm season, this results in 61% of
555 samples falling into the cold season compared with the warm season, which agrees well with the seasonal
556 precipitation climatology where conditions slightly favor cold season accumulation (e.g., about 60% of
557 snow occurs in the cold season on the coast; Laepple et al., 2011).

558 As illustrated in Fig. 7, snow $w(\text{NO}_3^-)$ spikes are present during the warm periods, while $w(\text{NO}_3^-)$ in the
559 cold season is lower. The averages of $w(\text{NO}_3^-)$ in warm and cold seasons are 62.0 and 36.6 ng g^{-1} ,
560 respectively (Fig. 8a). Previous observations at Antarctic coastal sites suggested that NO_3^- mass fractions
561 were generally higher in summer and lower in winter (Mulvaney et al., 1998; Wagenbach et al., 1998; Wolff
562 et al., 2008), which is consistent with our findings. In contrast, values of $\delta^{15}\text{N}$, $\delta^{18}\text{O}$ and $\Delta^{17}\text{O}$ of NO_3^- , are
563 all higher in cold seasons (with means of 31.0, 86.3 and 34.4‰, respectively); while the averages in warm
564 seasons are 15.1, 77.4 and 30.4‰, respectively (Fig. 8a).

565 Photolytic loss of NO_3^- at high accumulation sites such as Summit, Greenland (where the $200 \text{ kg m}^{-2} \text{ a}^{-1}$
566 accumulation rate is comparable to P1) appears to be negligible (Hastings et al., 2004; Fibiger et al., 2013).
567 In addition, the expected negative relationship between $w(\text{NO}_3^-)$ and $\delta^{15}\text{N}(\text{NO}_3^-)$ based upon the negative
568 photolytic $^{15}\epsilon$ (-45.3‰) is not observed nor does $\delta^{15}\text{N}(\text{NO}_3^-)$ show a sharp increase with the decreasing
569 $w(\text{NO}_3^-)$ in the upper 10 cm. Furthermore, given the results from the inland pits, a higher degree of
570 photolytic NO_3^- loss (i.e., the extent of photolysis) could be expected to be accompanied by more secondary
571 oxidation in the condensed phase (e.g., Jacobi and Hilker, 2007), leading to a decrease of $\delta^{18}\text{O}(\text{NO}_3^-)$ in the
572 upper snowpack. But there is a significant increasing trend of $\delta^{18}\text{O}(\text{NO}_3^-)$ in the upper 30 cm of snow (Fig. 7)
573 and there is no relationship between $\delta^{15}\text{N}(\text{NO}_3^-)$ and $\delta^{18}\text{O}(\text{NO}_3^-)$ in the dataset as a whole or when divided
574 by season. Thus, it is concluded that photolytic loss of NO_3^- at P1 is likely not influential.

575 If volatilization was driving the variability of $w(\text{NO}_3^-)$, a relationship between $w(\text{NO}_3^-)$ and $\delta^{15}\text{N}(\text{NO}_3^-)$
576 could be expected based on the theoretically calculated value for $^{15}\epsilon$ (Table S3), but none is observed (Table
577 2). On the other hand, the $^{15}\epsilon$ value at -20 °C reported from the Dome C experiment ($^{15}\epsilon=-0.3\text{‰}$) is
578 effectively non-fractionating (Erbland et al., 2013). Based on this, it is difficult to attribute the isotopic
579 variability in P1 to volatilization.

580 In summary, the observed variability in $w(\text{NO}_3^-)$ and isotopic composition cannot be explained by
581 post-depositional processes in snow, given our current knowledge of isotopic fractionations of the processes
582 discussed above. The observed large variations in the P1 isotopic and mass fraction data are more plausibly
583 explained as presenting a seasonal NO_3^- source shift over different periods (see below), which may be
584 further corroborated by the changing relationship of $w(\text{NO}_3^-)$ vs. $\delta^{18}\text{O}(\text{NO}_3^-)$ between cold and warm
585 seasons (Fig. 8b).

586 A number of studies have suggested that the stratosphere is the primary source of NO_3^- to the Antarctic
587 ice sheet (Mulvaney and Wolff, 1993; Wagenbach et al., 1998; Savarino et al., 2007), with an estimated
588 annual flux of $6.3\pm 2.7\times 10^7 \text{ kg N a}^{-1}$ (Muscarì et al., 2003). As discussed by Savarino et al. (2007),

589 interactions between NO_x and stratospheric ozone lead to some of the highest $\Delta^{17}\text{O}$ (and $\delta^{18}\text{O}$) of NO_3^-
590 values, which have thus far only been observed in polar regions. It is notable that $\delta^{18}\text{O}(\text{NO}_3^-)$ values above
591 90‰ are all present in cold season snow (Fig. 7), and $\delta^{18}\text{O}(\text{NO}_3^-)$ and $\Delta^{17}\text{O}(\text{NO}_3^-)$ (ranging from 69.5 to
592 105.3‰ and 25.2 to 42.9‰, respectively) in this period are comparable to the data of atmospheric NO_3^-
593 (inorganic NO_3^- aerosol) in winter at the coastal East Antarctic Dumont d'Urville station (DDU; 66°40'S,
594 140°01'E). At DDU, the higher $\delta^{18}\text{O}(\text{NO}_3^-)$ and $\Delta^{17}\text{O}(\text{NO}_3^-)$ in winter is thought to be linked with
595 stratospheric NO_3^- deposition (Savarino et al., 2007). The great enrichment of ^{18}O and ^{17}O in the cold season
596 NO_3^- in P1 suggests that O atoms from stratospheric O_3 have been incorporated into NO_x and NO_3^- (R4-R6)
597 that was subsequently deposited in snow as NO_3^- .

598 Interestingly, the highest $\delta^{18}\text{O}(\text{NO}_3^-)$ and $\Delta^{17}\text{O}(\text{NO}_3^-)$ values are all found in the most recent winter/spring
599 in P1, namely 2012. This season was marked by much less stratospheric O_3 loss and a smaller O_3 hole
600 extent than in previous seasons covered by the P1 snowpit; the mean 2012 O_3 hole area was 19% smaller
601 than the prior 3 year average, and the minimum O_3 concentration of 139.1DU detected by satellite was the
602 highest on record since 1988 (based on data from the NASA Goddard Space Flight Center:
603 http://ozonewatch.gsfc.nasa.gov/meteorology/annual_data.txt). This might support that, where atmospheric
604 NO_3^- is preserved in Antarctic snow, the O isotopes of NO_3^- could track stratospheric O_3 changes over time
605 (McCabe et al., 2007).

606 At South Pole, McCabe et al. (2007) suggested that the $\Delta^{17}\text{O}(\text{NO}_3^-)$ may track changes in stratospheric
607 ozone. However, McCabe et al. (2007) found an anti-correlation between $\Delta^{17}\text{O}(\text{NO}_3^-)$ with
608 October-December column ozone concentrations. Two hypotheses were proposed in this work: 1) the nitrate
609 oxygen isotopes are being primarily affected by increases in tropospheric ozone levels because of increased
610 UV from decreased springtime column ozone levels, or 2) the oxygen isotopes are recording increases in the
611 stratospheric nitrate flux during years of reduced column ozone. At South Pole, nitrate in snow is expected
612 to preserve only 25% of the original stratospheric isotopic composition, whereas 75% reflects the
613 tropospheric isotopic composition, due to nitrate produced locally from the snow-sourced, gas-phase
614 recycled NO_x on the polar plateau (McCabe et al., 2007). The situation is really different at coastal site P1,
615 where the photolysis imprint is rather minor. For snow nitrate in the cold season at P1, higher $\delta^{18}\text{O}(\text{NO}_3^-)$
616 and $\Delta^{17}\text{O}(\text{NO}_3^-)$ correspond to a smaller ozone hole (i.e., column ozone is higher) and this is most dramatic
617 in 2012.

618 The $\delta^{15}\text{N}(\text{NO}_3^-)$ in P1 cold season snow has a mean of $31.0 \pm 14.5\%$, which is much higher than that found
619 in atmospheric NO_3^- at DDU (maximum of 10.8‰). Savarino et al. (2007) calculated that the isotopic
620 signature of NO formed in the stratosphere would be $19 \pm 3\%$ based upon the estimated fractionation of N_2O
621 upon decomposition. Based on the expectation that more than 90% of stratospheric NO_y (sum of reactive
622 nitrogen oxide compounds) is removed during denitrification, Savarino et al. (2007) further predicted that
623 the $\delta^{15}\text{N}$ of NO is close to the $\delta^{15}\text{N}(\text{NO}_3^-)$. The much higher values found in coastal snow must then
624 represent either a higher stratospheric $\delta^{15}\text{N}$ source value than predicted, or fractionation associated with
625 chemistry, transport or deposition. The annual weighted average $\delta^{15}\text{N}(\text{NO}_3^-)$ in a skin layer of snow at the
626 air-snow interface was found to be 24.7‰ higher than that in atmospheric nitrate and it was suggested that
627 this was due to a fractionation associated with deposition (Erland et al., 2013). A striking difference
628 between $\delta^{18}\text{O}(\text{NO}_3^-)$ and $\Delta^{17}\text{O}(\text{NO}_3^-)$ in atmospheric nitrate and that in the skin layer was not found, and
629 instead the oxygen isotopes were suggested to be in equilibrium. The $\delta^{18}\text{O}(\text{NO}_3^-)$ in P1 and the correlation
630 of $\delta^{18}\text{O}(\text{NO}_3^-)$ and $\Delta^{17}\text{O}(\text{NO}_3^-)$ ($R^2=0.77$, $p<0.01$) fit well within the range expected for primary atmospheric
631 nitrate, and it is unlikely that significant fractionation associated with deposition (or chemistry or transport)
632 would affect only $\delta^{15}\text{N}(\text{NO}_3^-)$ and not $\delta^{18}\text{O}(\text{NO}_3^-)$. Thus, a higher $\delta^{15}\text{N}(\text{NO}_3^-)$ value (or range) than 19‰

633 from stratospheric denitrification is needed to explain the P1 cold season data.

634 The warm season snow in P1 exhibits lower mean $\delta^{15}\text{N}$, $\delta^{18}\text{O}$ and $\Delta^{17}\text{O}$ of NO_3^- (15.1, 77.4 and 30.4‰,
635 respectively). These lower values, and the occurrence of $\delta^{15}\text{N}(\text{NO}_3^-) < 0\text{‰}$ in warm seasons, are also
636 consistent with the DDU atmospheric data (Savarino et al., 2007). The very low and negative $\delta^{15}\text{N}(\text{NO}_3^-)$
637 values found between October-December at DDU were interpreted as resulting from HNO_3 formed in the
638 atmosphere from snow-sourced NO_x emissions transported from the plateau. Namely, the release of NO_x
639 from photolysis of surface snow NO_3^- can explain these values because of the very large and negative $^{15}\epsilon$
640 (see section 4.1.1 above). The seasonally lowered O isotopic composition can then be explained as arising
641 from the gas-phase oxidation of snow-sourced NO_x to HNO_3 predominantly by OH (R3), which would be
642 expected to be the predominant pathway of HNO_3 formation during the warm season (Alexander et al.,
643 2009).

644 While the mean values shown in Fig. 8a are representative of the seasonal shifts in the isotopic
645 composition of NO_3^- , it is also clear from Fig. 7 that there is significant interannual variability. A recent
646 adjoint modeling study suggested that $w(\text{NO}_3^-)$ in Antarctic snow was most sensitive to tropospheric sources
647 of NO_x , primarily fossil fuel combustion, biogenic soil emissions and lightning, though snow emissions
648 were not considered in the model (Lee et al., 2014). The isotopic signatures of NO_x sources and their
649 relationship with the $\delta^{15}\text{N}$ of NO_3^- are poorly constrained (e.g., Fibiger et al., 2014), particularly in the
650 Southern Hemisphere. For example, the $\delta^{15}\text{N}$ of NO_x from vehicle emissions in South Africa were
651 consistently negative (Heaton, 1990) while that found in Switzerland was mostly positive (Ammann et al.,
652 1999) and a recent study in the U.S. suggests very positive values associated with vehicle emissions (Felix
653 and Elliott, 2014). Natural, biogenic soil emissions have not been directly quantified, but fertilized soils in a
654 laboratory study emitted NO_x with very low $\delta^{15}\text{N}$ (from -48.9 to -19.9 ‰) (Li and Wang, 2008), and
655 lightning-sourced NO_x is expected to be near 0‰. Additionally, peroxyacetyl nitrate (PAN) is suggested as
656 an important source of NO_x to the Antarctic atmosphere during the warm season (Lee et al., 2014). While no
657 direct information is available in terms of the $\delta^{15}\text{N}$ of NO_x (or NO_3^-) produced from PAN decomposition, it
658 has been suggested that this could explain sporadic high $\delta^{15}\text{N}$ of NO_3^- in the northern subtropical marine
659 system (Altieri et al., 2013). It is not possible at this time to link the observed changes in isotopic
660 composition directly to NO_x emission sources. Still, qualitatively, and based on the combination of isotopes,
661 the P1 snowpit data would agree with a varying relative contribution of tropospheric NO_x sources from
662 year-to-year in the warm season. In the cold season, the data suggest that there is still an important degree of
663 stratospheric influence on NO_3^- loading in Antarctic snow, particularly in 2012 when the O_3 hole was
664 unusually small.

665

666 5 Conclusion

667

668 The purpose of this study was to investigate the effects of post-depositional processes on isotopic
669 fractionation of NO_3^- at different depths in the snowpack, and to understand variation of NO_3^- isotopic
670 composition in different environments on the EAIS. In the EAIS interior, where accumulation rates are very
671 low (group II snowpits; $< 55 \text{ kg m}^{-2} \text{ a}^{-1}$), a high degree of NO_3^- loss is found. The high values of $\delta^{15}\text{N}(\text{NO}_3^-)$
672 found in near-surface snow (i.e., top 20 cm) and the relationship between $w(\text{NO}_3^-)$ and $\delta^{15}\text{N}(\text{NO}_3^-)$ are
673 consistent with a Rayleigh-type process and theoretically predicted $^{15}\epsilon$ values for NO_3^- photolysis. The
674 concurrent decreases in $\delta^{18}\text{O}(\text{NO}_3^-)$, however, are best explained as resulting from condensed-phase
675 re-oxidation forming secondary NO_3^- that contains oxygen atoms derived from in situ H_2O (e.g., $\delta^{18}\text{O}(\text{H}_2\text{O})$
676 of -50‰). This significantly decreases the $\delta^{18}\text{O}(\text{NO}_3^-)$ overall from what was originally deposited, and

677 explains the positive relationship between $w(\text{NO}_3^-)$ and the $\delta^{18}\text{O}$ of NO_3^- (and therefore the positive
678 observed $^{18}\epsilon_{app}$ values). Interestingly, below 20 cm in the group II snowpits, a change in the relationship
679 between $w(\text{NO}_3^-)$ and $\delta^{18}\text{O}(\text{NO}_3^-)$ is observed. These findings highlight the utility of the combined use of
680 $\delta^{15}\text{N}(\text{NO}_3^-)$ and $\delta^{18}\text{O}(\text{NO}_3^-)$ for detecting post-depositional processing of NO_3^- and the difficulty in
681 predicting the isotopic composition of NO_3^- at depth based on the fractionation of near-surface NO_3^- alone.
682 We find that in both group II and group I snowpits (accumulation $>91 \text{ kg m}^{-2} \text{ a}^{-1}$), $w(\text{NO}_3^-)$, $\delta^{15}\text{N}(\text{NO}_3^-)$, and
683 $\delta^{18}\text{O}(\text{NO}_3^-)$ cannot be fit by a simple exponential decrease model, implying that photolytic loss cannot be
684 assumed to operate consistently over time. In the case of the group II snowpits, a significant negative
685 relationship is observed between $w(\text{NO}_3^-)$ and $\delta^{18}\text{O}(\text{NO}_3^-)$ at depths between 100-200 cm. We suggest that
686 the change over time in the behavior of the isotopes is best explained as being driven by changes in the
687 photolability of nitrate and thus, chemistry of the snow. In the case of the group I snowpits, seasonal
688 variability is found in $w(\text{NO}_3^-)$, $\delta^{15}\text{N}$, $\delta^{18}\text{O}$, and $\Delta^{17}\text{O}$ of NO_3^- throughout the profiles. We suggest that the
689 seasonality observed in higher accumulation, more coastal EAIS sites is driven by the influence of seasonal
690 changes in NO_3^- sources. The best explanation for the range of values seen, given current knowledge, is the
691 importance of stratospheric production of atmospheric NO_3^- in the cold season compared to more
692 tropospheric NO_x source influence in the warm season.

693

694 **Supplementary material related to this article is attached.**

695

696 *Acknowledgements.* This research was supported by the National Science Foundation of China (Grant Nos.
697 41206188 to GS, 41476169 to SJ), the U.S. National Science Foundation Antarctic Glaciology Program
698 (Grant No. 1246223 to MGH) and Chinese Polar Environment Comprehensive Investigation and
699 Assessment Programmes (Grant Nos. CHINARE 2014-02-02 to BS, 2014-04-01 to GS). We are also
700 grateful to Ruby Ho at Brown University and the 29th CHINARE inland members for technical support and
701 assistance, and Dr. Erbland and two anonymous reviewers for their helpful comments.

702

703 **References**

704

- 705 Alexander, B., Savarino, J., Kreutz, K. J., and Thiemens, M.: Impact of preindustrial biomass-burning
706 emissions on the oxidation pathways of tropospheric sulfur and nitrogen, *J. Geophys. Res.*, 109, D08303,
707 doi:10.1029/2003JD004218, 2004.
- 708 Alexander, B., Hastings, M., Allman, D., Dachs, J., Thornton, J., and Kunasek, S.: Quantifying atmospheric
709 nitrate formation pathways based on a global model of the oxygen isotopic composition ($\Delta^{17}\text{O}$) of
710 atmospheric nitrate, *Atmos. Chem. Phys.*, 9, 5043-5056, 2009.
- 711 Altieri, K., Hastings, M., Gobel, A., Peters, A., and Sigman, D.: Isotopic composition of rainwater nitrate at
712 Bermuda: The influence of air mass source and chemistry in the marine boundary layer, *J. Geophys.*
713 *Res.*, 118, 11304-11316, 2013.
- 714 Ammann, M., Siegwolf, R., Pichlmayer, F., Suter, M., Saurer, M., and Brunold, C.: Estimating the uptake of
715 traffic-derived NO_2 from ^{15}N abundance in Norway spruce needles, *Oecologia*, 118, 124-131, 1999.
- 716 Böhlke, J., Mroczkowski, S., and Coplen, T.: Oxygen isotopes in nitrate: New reference materials for ^{18}O :
717 ^{17}O : ^{16}O measurements and observations on nitrate-water equilibration, *Rapid Commun. Mass.*
718 *Spectrom.*, 17, 1835-1846, 2003.
- 719 Berhanu, T. A., Meusinger, C., Erbland, J., Jost, R., Bhattacharya, S., Johnson, M. S., and Savarino, J.:
720 Laboratory study of nitrate photolysis in Antarctic snow. II. Isotopic effects and wavelength dependence,

721 J. Chem. Phys., 140, 244306, doi:10.1063/1.4882899, 2014.

722 Blunier, T., Floch, G., Jacobi, H.-W., and Quansah, E.: Isotopic view on nitrate loss in Antarctic surface
723 snow, *Geophys. Res. Lett.*, 32, L13501, doi:10.1029/2005GL023011, 2005.

724 Boxe, C., Colussi, A., Hoffmann, M., Murphy, J., Wooldridge, P., Bertram, T., and Cohen, R.:
725 Photochemical production and release of gaseous NO₂ from nitrate-doped water ice, *J. Phys. Chem.*, 109,
726 8520-8525, 2005.

727 Buffen, A. M., Hastings, M. G., Thompson, L. G., and Mosley-Thompson, E.: Investigating the preservation
728 of nitrate isotopic composition in a tropical ice core from the Quelccaya Ice Cap, Peru, *J. Geophys. Res.*,
729 119, 2674-2697, doi: 10.1002/2013JD020715, 2014.

730 Bunton, C., Halevi, E., and Llewellyn, D.: Oxygen exchange between nitric acid and water. Part I, *J. Chem.*
731 *Soc.*, 4913-4916, doi:10.1039/jr9520004913, 1952.

732 Casciotti, K., Sigman, D., Hastings, M. G., Böhlke, J., and Hilkert, A.: Measurement of the oxygen isotopic
733 composition of nitrate in seawater and freshwater using the denitrifier method, *Anal. Chem.*, 74,
734 4905-4912, 2002.

735 Chu, L., and Anastasio, C.: Quantum yields of hydroxyl radical and nitrogen dioxide from the photolysis of
736 nitrate on ice, *J. Phys. Chem.*, 107, 9594-9602, 2003.

737 Criss, R. E.: *Principles of stable isotope distribution*, Oxford University Press, New York, 254 pp., 1999.

738 Davis, D. D., Seelig, J., Huey, G., Crawford, J., Chen, G., Wang, Y., Buhr, M., Helmig, D., Neff, W., Blake,
739 D., Arimot, R., and Eisele, F.: A reassessment of Antarctic plateau reactive nitrogen based on ANTCI
740 2003 airborne and ground based measurements, *Atmos. Environ.*, 42, 2831-2848, 2008.

741 Delmas, R., Serca, D., and Jambert, C.: Global inventory of NO_x sources, *Nutr. Cycl. Agroecosys.*, 48, 51-60,
742 1997.

743 Dibb, J. E., Arsenault, M., Peterson, M. C., and Honrath, R. E.: Fast nitrogen oxide photochemistry in
744 Summit, Greenland snow, *Atmos. Environ.*, 36, 2501-2511, 2002.

745 Dibb, J. E., and Fahnestock, M.: Snow accumulation, surface height change, and firn densification at
746 Summit, Greenland: Insights from 2 years of in situ observation, *J. Geophys. Res.*, 109, D24113, doi:
747 10.1029/2003JD004300, 2004.

748 Ding, M., Xiao, C., Jin, B., Ren, J., Qin, D., and Sun, W.: Distribution of $\delta^{18}\text{O}$ in surface snow along a
749 transect from Zhongshan Station to Dome A, East Antarctica, *Chin. Sci. Bull.*, 55, 2709-2714, 2010.

750 Ding, M., Xiao, C., Li, Y., Ren, J., Hou, S., Jin, B., and Sun, B.: Spatial variability of surface mass balance
751 along a traverse route from Zhongshan station to Dome A, Antarctica, *J. Glaciol.*, 57, 658-666, 2011.

752 Dubowski, Y., Colussi, A., and Hoffmann, M.: Nitrogen dioxide release in the 302 nm band photolysis of
753 spray-frozen aqueous nitrate solutions. Atmospheric implications, *J. Phys. Chem.*, 105, 4928-4932,
754 2001.

755 Elliott, E. M., Kendall, C., Wankel, S. D., Burns, D. A., Boyer, E. W., Harlin, K., Bain, D. J., and Butler, T.
756 J.: Nitrogen isotopes as indicators of NO_x source contributions to atmospheric nitrate deposition across
757 the midwestern and northeastern United States, *Environ. Sci. Technol.*, 41, 7661-7667,
758 10.1021/es070898t, 2007.

759 Erbland, J., Vicars, W., Savarino, J., Morin, S., Frey, M., Frosini, D., Vince, E., and Martins, J.: Air-snow
760 transfer of nitrate on the East Antarctic Plateau - Part 1: Isotopic evidence for a photolytically driven
761 dynamic equilibrium in summer, *Atmos. Chem. Phys.*, 13, 6403-6419, 2013.

762 Felix, J. D., and Elliott, E. M.: Isotopic composition of passively collected nitrogen dioxide emissions:
763 Vehicle, soil and livestock source signatures, *Atmos. Environ.*, 92, 359-366, 2014.

764 Fibiger, D. L., Hastings, M. G., Dibb, J. E., and Huey, L. G.: The preservation of atmospheric nitrate in

765 snow at Summit, Greenland, *Geophys. Res. Lett.*, 40, 3484-3489, 2013.

766 Frey, M. M., Brough, N., France, J. L., Anderson, P. S., Traulle, O., King, M. D., Jones, A. E., Wolff, E. W.,
767 and Savarino, J.: The diurnal variability of atmospheric nitrogen oxides (NO and NO₂) above the
768 Antarctic Plateau driven by atmospheric stability and snow emissions, *Atmos. Chem. Phys.*, 13,
769 3045-3062, 2013.

770 Frey, M. M., Savarino, J., Morin, S., Erbland, J., and Martins, J.: Photolysis imprint in the nitrate stable
771 isotope signal in snow and atmosphere of East Antarctica and implications for reactive nitrogen cycling,
772 *Atmos. Chem. Phys.*, 9, 8681-8696, 2009.

773 Grannas, A., Jones, A. E., Dibb, J., Ammann, M., Anastasio, C., Beine, H., Bergin, M., Bottenheim, J., Boxe,
774 C., and Carver, G.: An overview of snow photochemistry: evidence, mechanisms and impacts, *Atmos.*
775 *Chem. Phys.*, 7, 4329-4373, 2007.

776 Hastings, M. G., Sigman, D. M., and Lipschultz, F.: Isotopic evidence for source changes of nitrate in rain at
777 Bermuda, *J. Geophys. Res.*, 108, 4790, doi:10.1029/2003JD003789, 2003.

778 Hastings, M. G., Steig, E., and Sigman, D.: Seasonal variations in N and O isotopes of nitrate in snow at
779 Summit, Greenland: Implications for the study of nitrate in snow and ice cores, *J. Geophys. Res.*, 109,
780 D20306, doi:10.1029/2004JD004991, 2004.

781 Hastings, M. G., Jarvis, J. C., and Steig, E. J.: Anthropogenic impacts on nitrogen isotopes of ice-core
782 nitrate, *Science*, 324, 1288-1288, 2009.

783 Hastings, M. G.: Evaluating source, chemistry and climate change based upon the isotopic composition of
784 nitrate in ice cores, IOP Conference Series: Earth and Environmental Science,
785 9,012002,doi:10.1088/1755-1315/9/1/012002, 2010.

786 Heaton, T. H. E.: ¹⁵N/¹⁴N ratios of NO_x from vehicle engines and coal-fired power stations, *Tellus. B*, 42,
787 304-307, 1990.

788 Jacobi, H.-W., and Hilker, B.: A mechanism for the photochemical transformation of nitrate in snow, *J.*
789 *Photochem. Photobiol. A*, 185, 371-382, 2007.

790 Johnsen, S. J., Clausen, H. B., Dansgaard, W., Gundestrup, N. S., Hammer, C. U., Andersen, U., Andersen,
791 K. K., Hvidberg, C. S., Dahl-Jensen, D., and Steffensen, J. P.: The δ¹⁸O record along the Greenland Ice
792 Core Project deep ice core and the problem of possible Eemian climatic instability, *J. Geophys. Res.*,
793 102, 26397-26410, 1997.

794 Kaiser, J., Hastings, M. G., Houlton, B. Z., Röckmann, T., and Sigman, D. M.: Triple oxygen isotope
795 analysis of nitrate using the denitrifier method and thermal decomposition of N₂O, *Anal. Chem.*, 79,
796 599-607, 2007.

797 Laepple, T., Werner, M., and Lohmann, G.: Synchronicity of Antarctic temperatures and local solar
798 insolation on orbital timescales, *Nature*, 471, 91-94, 2011.

799 Lee, D., Köhler, I., Grobler, E., Rohrer, F., Sausen, R., Gallardo-Klenner, L., Olivier, J., Dentener, F., and
800 Bouwman, A.: Estimations of global NO_x emissions and their uncertainties, *Atmos. Environ.*, 31,
801 1735-1749, 1997.

802 Lee, H.-M., Henze, D. K., Alexander, B., and Murray, L. T.: Investigating the sensitivity of surface-level
803 nitrate seasonality in Antarctica to primary sources using a global model, *Atmos. Environ.*, 89, 757-767,
804 2014.

805 Li, D., and Wang, X.: Nitrogen isotopic signature of soil-released nitric oxide (NO) after fertilizer
806 application, *Atmos. Environ.*, 42, 4747-4754, 2008.

807 Madronich, S., and Flocke, S.: The role of solar radiation in atmospheric chemistry, in: *Handbook of*
808 *Environmental Chemistry*, edited by: Boule, P., Springer Verlag, Heidelberg, 1-26, 1998.

809 Mayewski, P. A., and Legrand, M. R.: Recent increase in nitrate concentration of Antarctic snow, *Nature*,
810 346, 258-260, 1990.

811 McCabe, J., Boxe, C., Colussi, A., Hoffmann, M., and Thiemens, M.: Oxygen isotopic fractionation in the
812 photochemistry of nitrate in water and ice, *J. Geophys. Res.*, 110, D15310, doi:10.1029/2004JD005484,
813 2005.

814 McCabe, J. R., Thiemens, M. H., and Savarino, J.: A record of ozone variability in South Pole Antarctic
815 snow: Role of nitrate oxygen isotopes, *J. Geophys. Res.*, 112, D12303, doi:10.1029/2006JD007822,
816 2007.

817 Meusinger, C., Berhanu, T. A., Erbland, J., Savarino, J., and Johnson, M. S.: Laboratory study of nitrate
818 photolysis in Antarctic snow. I. Observed quantum yield, domain of photolysis, and secondary chemistry,
819 *J. Chem. Phys.*, 140, 244305, doi: 10.1063/1.4882898, 2014.

820 Michalski, G., Savarino, J., Böhlke, J., and Thiemens, M.: Determination of the total oxygen isotopic
821 composition of nitrate and the calibration of a $\Delta^{17}\text{O}$ nitrate reference material, *Anal. Chem.*, 74,
822 4989-4993, 2002.

823 Michalski, G., Scott, Z., Kabling, M., and Thiemens, M. H.: First measurements and modeling of $\Delta^{17}\text{O}$ in
824 atmospheric nitrate, *Geophys. Res. Lett.*, 30, 1870, doi: 10.1029/2003GL017015, 2003.

825 Morin, S., Savarino, J., Frey, M. M., Yan, N., Bekki, S., Bottenheim, J. W., and Martins, J. M.: Tracing the
826 origin and fate of NO_x in the Arctic atmosphere using stable isotopes in nitrate, *Science*, 322, 730-732,
827 2008.

828 Mulvaney, R., and Wolff, E.: Evidence for winter/spring denitrification of the stratosphere in the nitrate
829 record of Antarctic firn cores, *J. Geophys. Res.*, 98, 5213-5220, 1993.

830 Mulvaney, R., Wagenbach, D., and Wolff, E. W.: Postdepositional change in snowpack nitrate from
831 observation of year-round near-surface snow in coastal Antarctica, *J. Geophys. Res.*, 103, 11021-11031,
832 1998.

833 Muscari, G., de Zafra, R. L., and Smyshlyaev, S.: Evolution of the NO_y - N_2O correlation in the Antarctic
834 stratosphere during 1993 and 1995, *J. Geophys. Res.*, 108, 4428, doi:10.1029/2002JD002871, 2003.

835 Röthlisberger, R., Hutterli, M. A., Sommer, S., Wolff, E. W., and Mulvaney, R.: Factors controlling nitrate in
836 ice cores: Evidence from the Dome C deep ice core, *J. Geophys. Res.*, 105, 20565-20572, 2000.

837 Röthlisberger, R., Hutterli, M. A., Wolff, E. W., Mulvaney, R., Fischer, H., Bigler, M., Goto-Azuma, K.,
838 Hansson, M. E., Ruth, U., and Siggaard-Andersen, M.-L.: Nitrate in Greenland and Antarctic ice cores:
839 A detailed description of post-depositional processes, *Ann. Glaciol.*, 35, 209-216, 2002.

840 Sato, K., Takenaka, N., Bandow, H., and Maeda, Y.: Evaporation loss of dissolved volatile substances from
841 ice surfaces, *J. Phys. Chem.*, 112, 7600-7607, 2008.

842 Savarino, J., Kaiser, J., Morin, S., Sigman, D. M., and Thiemens, M. H.: Nitrogen and oxygen isotopic
843 constraints on the origin of atmospheric nitrate in coastal Antarctica, *Atmos. Chem. Phys.*, 7, 1925-1945,
844 2007.

845 Sigman, D. M., Casciotti, K. L., Andreani, M., Barford, C., Galanter, M., and Böhlke, J. K.: A bacterial
846 method for the nitrogen isotopic analysis of nitrate in seawater and freshwater, *Anal. Chem.*, 73,
847 4145-4153, 2001.

848 Traversi, R., Becagli, S., Castellano, E., Cerri, O., Morganti, A., Severi, M., and Udisti, R.: Study of Dome
849 C site (East Antarctica) variability by comparing chemical stratigraphies, *Microchem. J.*, 92, 7-14, 2009.

850 Wang, Y., Sodemann, H., Hou, S., Masson-Delmotte, V., Jouzel, J., and Pang, H.: Snow accumulation and
851 its moisture origin over Dome Argus, Antarctica, *Clim. Dynam.*, 40, 731-742, doi:
852 10.1007/s00382-012-1398-9, 2013.

853 Wagenbach, D., Graf, V., Minikin, A., Trefzer, U., Kipfstuhl, J., Oerter, H., and Blindow, N.:
854 Reconnaissance of chemical and isotopic firn properties on top of Berkner Island, Antarctica, *Ann.*
855 *Glaciol.*, 20, 307-312, 1994.

856 Wagenbach, D., Legrand, M., Fischer, H., Pichlmayer, F., and Wolff, E. W.: Atmospheric near-surface
857 nitrate at coastal Antarctic sites, *J. Geophys. Res.*, 103, 11007-11020, 1998.

858 Warneck, P., and Wurzinger, C.: Product quantum yields for the 305-nm photodecomposition of nitrate in
859 aqueous solution, *J. Phys. Chem.*, 92, 6278-6283, 1988.

860 Warren, S. G., Brandt, R. E., and Grenfell, T. C.: Visible and near-ultraviolet absorption spectrum of ice
861 from transmission of solar radiation into snow, *Appl. Optics*, 45, 5320-5334, 2006.

862 Wolff, E. W.: Nitrate in polar ice, in: in *Ice core studies of global biogeochemical cycles*, edited by: Delmas,
863 R. J., Springer, New York, 195-224, 1995.

864 Wolff, E. W., Jones, A. E., Bauguitte, S.-B., and Salmon, R. A.: The interpretation of spikes and trends in
865 concentration of nitrate in polar ice cores, based on evidence from snow and atmospheric measurements,
866 *Atmos. Chem. Phys.*, 8, 5627-5634, 2008.

867 Wolff, E. W., Bigler, M., Curran, M., Dibb, J., Frey, M., Legrand, M., and McConnell, J.: The Carrington
868 event not observed in most ice core nitrate records, *Geophys. Res. Lett.*, 39, L08503,
869 doi:10.1029/2012GL051603, 2012.

870 Xiao, C., Ding, M., Masson-Delmotte, V., Zhang, R., Jin, B., Ren, J., Li, C., Werner, M., Wang, Y., and Cui,
871 X.: Stable isotopes in surface snow along a traverse route from Zhongshan station to Dome A, East
872 Antarctica, *Clim. Dynam.*, 41, 2427-2438, 2013.

873 Yung, Y. L., and Miller, C. E.: Isotopic fractionation of stratospheric nitrous oxide, *Science*, 278, 1778-1780,
874 doi:10.1126/ science.278.5344.1778., 1997.

875 Zatko, M., Grenfell, T., Alexander, B., Doherty, S., Thomas, J., and Yang, X.: The influence of snow grain
876 size and impurities on the vertical profiles of actinic flux and associated NO_x emissions on the Antarctic
877 and Greenland ice sheets, *Atmos. Chem. Phys.*, 13, 3547-3567, 2013.

878
879
880

881 Table 1. Summary information for the seven snowpits presented in this study.

Snowpit	Location	Elevation, m	Distance from coast, km	Mean annual accumulation, kg m ⁻² a ⁻¹ 1)	Mean annual Temperature, °C 2)	Depth, cm	Sampling resolution, cm	Sampling date, DD.MM.YYYY
P1	71.13°S, 77.31°E	2037	200	172.0	-29.12	150	3.0	18.12.2012
P2	71.81°S, 77.89°E	2295	283	99.4	-32.87	200	5.0	20.12.2012
P3	73.40°S, 77.00°E	2545	462	90.7	-35.72	200	5.0	22.12.2012
P4	76.29°S, 77.03°E	2843	787	54.8	-41.28	200	2.0	28.12.2012
P5	77.91°S, 77.13°E	3154	968	33.3	-46.37	200	2.0	30.12.2012
P6	79.02°S, 76.98E	3738	1092	25.4	-53.13	200	2.5	02.01.2013
P7	80.42°S, 77.12°E	4093	1256	23.5	-58.50	300	2.5	06.01.2013

882 1) Mean annual snow accumulation rates are obtained from bamboo stick field measurements, updated to
883 2013 from Ding et al. (2011).

884 2) Mean annual temperatures are derived from 10m borehole temperatures and automatic weather station
885 observations (Ding et al., 2010; Xiao et al., 2013).

886

887

888 Table 2. Observed fractionation constants for ^{15}N and ^{18}O of NO_3^- ($^{15}\epsilon_{\text{app}}$ and $^{18}\epsilon_{\text{app}}$) calculated for different
 889 snow layer depths from the linear regression of $\ln(\delta_{\text{snow}}+1)$ vs. $\ln(w_{\text{snow}})$ in Eq. (2). Four different depth
 890 intervals were selected for calculating ϵ_{app} : 0-20cm, 0-40cm, 0-60cm, 100-bottom and the entire pit. Also
 891 given are the standard error (1σ), r^2 values and the significance level, p , where bolded values represent $p <$
 892 0.05.

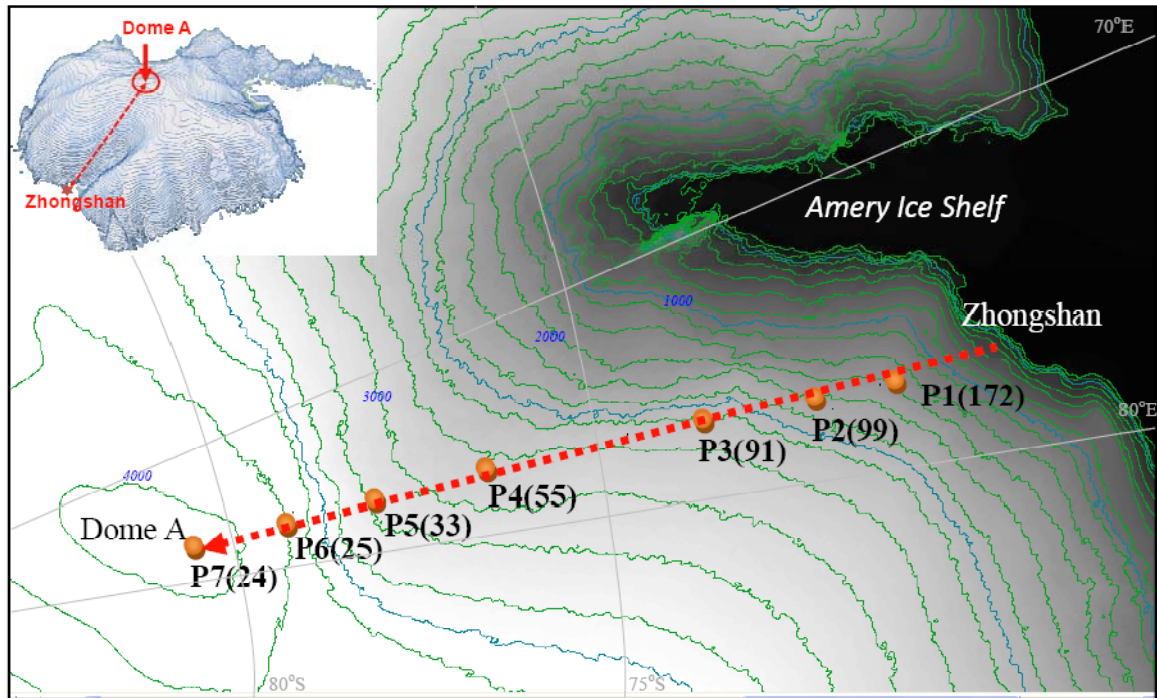
Snow pit	Depth	^{15}N			^{18}O		
		$^{15}\epsilon_{\text{app}} \pm 1\sigma, \text{‰}$	p	r^2	$^{18}\epsilon_{\text{app}} \pm 1\sigma, \text{‰}$	p	r^2
P1	0-20cm	2.4±2.0	0.379	0.157	-15.3±6.0	0.044	0.588
	0-40cm	-0.4±5.0	0.943	0.000	-8.7±7.0	0.248	0.109
	0-60cm	-3.9±14.0	0.785	0.004	-9.4±10.0	0.368	0.043
	100-Bottom	17.2±14.0	0.248	0.094	-6.5±5.0	0.175	0.127
	Entire	-11.8±7.0	0.098	0.056	-3.7±4.0	0.390	0.015
P2	0-20cm	-45.5±26.0	0.184	0.497	4.0±1.0	0.017	0.887
	0-40cm	0.8±10.0	0.936	0.001	-4.2±4.0	0.274	0.167
	0-60cm	4.1±15.0	0.789	0.007	-2.1±4.0	0.647	0.020
	100-Bottom	21.5±16.0	0.197	0.091	11.2±4.2	0.015	0.287
	Entire	11.9±9.1	0.198	0.043	7.0±3.6	0.060	0.090
P3	0-20cm	-36.8±6.7	0.012	0.909	-19.8±13.5	0.237	0.420
	0-40cm	-27.5±11.0	0.036	0.488	-15.4±11.0	0.188	0.233
	0-60cm	-28.8±9.1	0.009	0.476	-14.0±8.7	0.135	0.192
	100-Bottom	12.3±12.0	0.318	0.059	13.5±18.6	0.478	0.030
	Entire	-1.2±4.9	0.811	0.002	15.4±8.0	0.061	0.092
P4	0-20cm	-77.8±9.2	0.000	0.888	17.1±3.1	0.000	0.778
	0-40cm	-81.6±7.5	0.000	0.868	14.0±2.1	0.000	0.706
	0-60cm	-73.3±9.8	0.000	0.665	11.4±2.5	0.000	0.419
	100-Bottom	-56.0±5.3	0.000	0.703	-3.4±1.3	0.011	0.126
	Entire	-58.7±5.0	0.000	0.584	1.4±1.8	0.433	0.006
P5	0-20cm	-93.1±23.6	0.003	0.633	30.2±12.3	0.036	0.401
	0-40cm	-92.1±10.8	0.000	0.791	24.9±5.5	0.000	0.522
	0-60cm	-92.5±8.1	0.000	0.820	16.0±3.6	0.000	0.412
	100-Bottom	27.3±13.7	0.053	0.083	-9.6±4.0	0.022	0.114
	Entire	-56.9±5.0	0.000	0.577	0.0±1.6	0.985	0.000
P6	0-20cm	-50.2±7.3	0.000	0.889	16.7±5.1	0.017	0.638
	0-40cm	-63.0±21.0	0.010	0.390	16.2±12.1	0.201	0.114
	0-60cm	-70.8±25.1	0.010	0.265	17.9±9.3	0.066	0.145
	100-Bottom	-61.3±8.0	0.000	0.605	-7.8±2.4	0.003	0.216
	Entire	-76.8±5.8	0.000	0.694	11.3±2.1	0.000	0.265
P7	0-20cm	-61.3±9.8	0.000	0.849	18.4±4.1	0.003	0.738
	0-40cm	-73.9±8.5	0.000	0.834	16.4±2.4	0.000	0.753
	0-60cm	-81.0±8.7	0.000	0.789	15.2±1.9	0.000	0.728
	100-Bottom	20.7±14.4	0.154	0.026	10.0±4.5	0.051	0.060
	Entire	-31.5±5.0	0.000	0.251	-0.7±1.7	0.690	0.001

893

894 Table 3. Asymptotic values of $w(\text{NO}_3^-)$, $\delta^{15}\text{N}$ and $\delta^{18}\text{O}$ of NO_3^- calculated based on four different snow
895 depth intervals (0-20cm, 0-40cm, 0-60cm and 0-100cm) of each snowpit. p is the significance level of
896 observed data fitted using the exponential decrease regression Eq. (6), and r^2 denotes squared correlation
897 coefficient of observed data compared to the regression model predicted values. Also given is the standard
898 error (1σ) of asymptotic values.

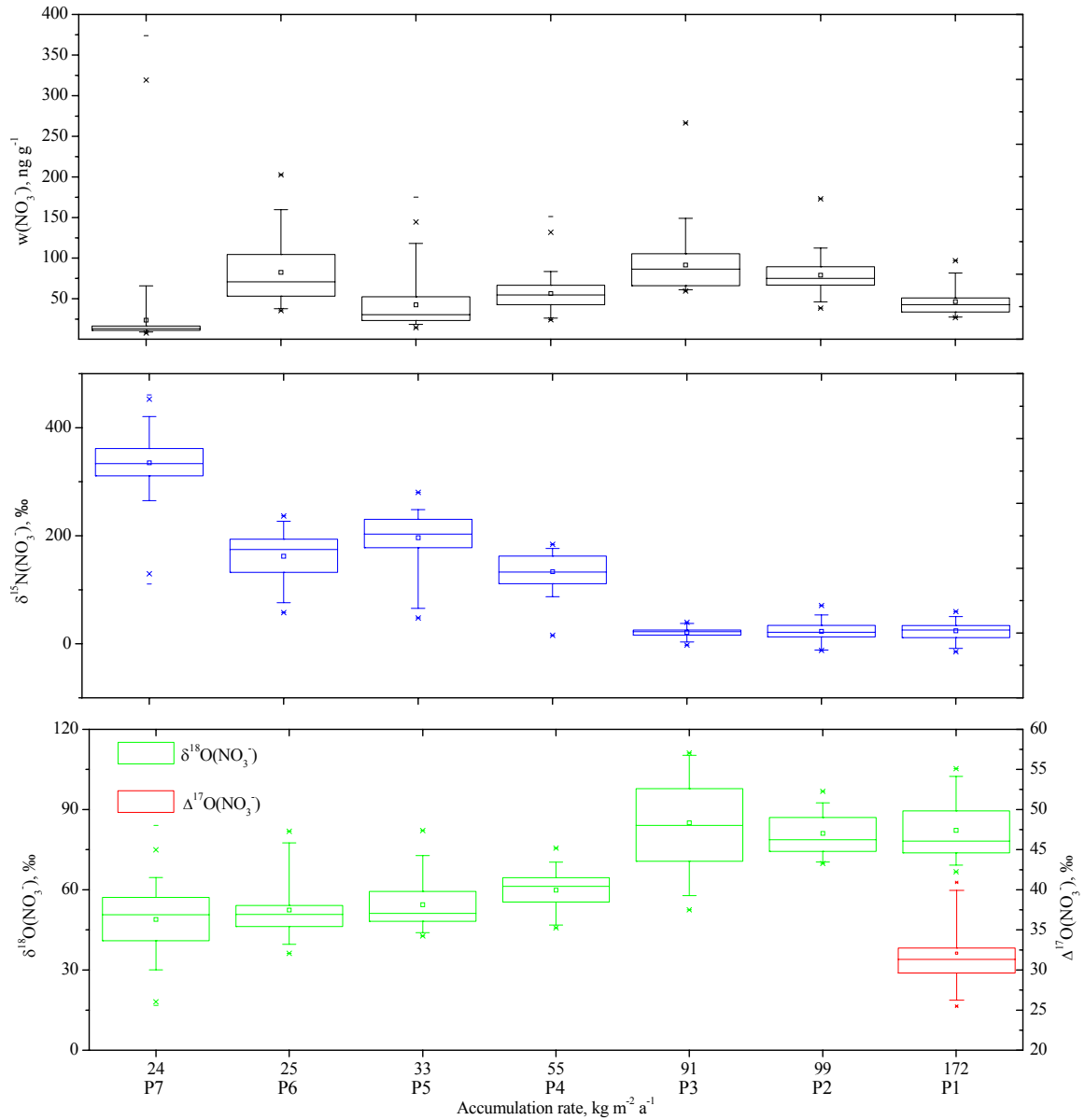
Snowpit	Depth	$w(\text{NO}_3^-)_{(\text{as.})}$, ng g ⁻¹			$\delta^{15}\text{N}_{(\text{as.})}$, ‰			$\delta^{18}\text{O}_{(\text{as.})}$, ‰		
		$w(\text{NO}_3^-) \pm 1\sigma$	p	r^2	$\delta^{15}\text{N} \pm 1\sigma$	p	r^2	$\delta^{18}\text{O} \pm 1\sigma$	p	r^2
P4	0-20cm	26.9±15.7	0.00	0.92	165.4±18.3	0.00	0.94	41.2±7.4	0.00	0.88
	0-40cm	38.1±3.5	0.00	0.92	173.2±5.4	0.00	0.95	49.2±1.3	0.00	0.80
	0-60cm	45.3±2.7	0.00	0.83	158.4±4.3	0.00	0.82	51.6±1.1	0.00	0.58
	0-100cm	54.5±2.5	0.00	0.58	144.3±3.9	0.00	0.51	54.5±0.9	0.00	0.29
P5	0-20cm	50.0±4.3	0.00	0.82	166.2±6.5	0.00	0.74	41.6±3.1	0.00	0.63
	0-40cm	39.6±13.5	0.00	0.91	216.6±58.7	0.00	0.95	43.5±4.1	0.00	0.80
	0-60cm	39.9±6.1	0.00	0.92	277.9±51.2	0.00	0.89	46.0±1.8	0.00	0.71
	0-100cm	25.8±3.3	0.00	0.93	254.6±10.6	0.00	0.92	48.2±1.0	0.00	0.65
P6	0-20cm	101.3±32.9	0.00	0.73	106.4±11.1	0.09	0.43	63.4±38.4	0.20	0.26
	0-40cm	131.1±7.7	0.01	0.45	95.2±7.4	0.45	0.04	48.3±105.6	0.03	0.29
	0-60cm	121.4±6.7	0.00	0.39	160.1±196.8	0.00	0.42	22.7±15.0	0.00	0.54
	0-100cm	40.4±3.6	0.00	0.65	179.7±54.5	0.00	0.43	39.9±7.4	0.00	0.61
P7	0-20cm	15.7±26.9	0.00	0.96	298.7±40.5	0.00	0.85	29.2±18.5	0.00	0.73
	0-40cm	22.3±6.9	0.00	0.97	490.0±23.0	0.00	0.90	23.2±7.0	0.00	0.78
	0-60cm	23.3±3.9	0.00	0.97	448.7±33.1	0.00	0.86	29.7±2.5	0.00	0.75
	0-100cm	17.9±2.3	0.00	0.97	383.8±9.4	0.00	0.75	33.9±1.4	0.00	0.64

899
900
901
902
903



904

905 Fig. 1. Snowpit locations sampled during the 2012/2013 Chinese National Antarctic Research Expedition
 906 (CHINARE) inland traverse. The numbers in parentheses denote the annual snow accumulation rates (kg
 907 m⁻² a⁻¹) which are extended to 2013 from bamboo stick field measurements (Ding et al., 2011).
 908



909

910 Fig. 2. Statistics of mass fraction and isotopic compositions of NO_3^- for each snowpit (P1-P7), plotted as a
 911 function of snow accumulation rate. Box and whisker plots represent maximum (top x symbol for each box),
 912 minimum (bottom x symbol for each box), percentiles (5th, 25th, 75th, and 95th), and median (50th, solid line)
 913 and mean (open square near center of each box). It is noted that the data of $\Delta^{17}\text{O}(\text{NO}_3^-)$ are only available
 914 for P1 pit.

915

916

917

918

919

920

921

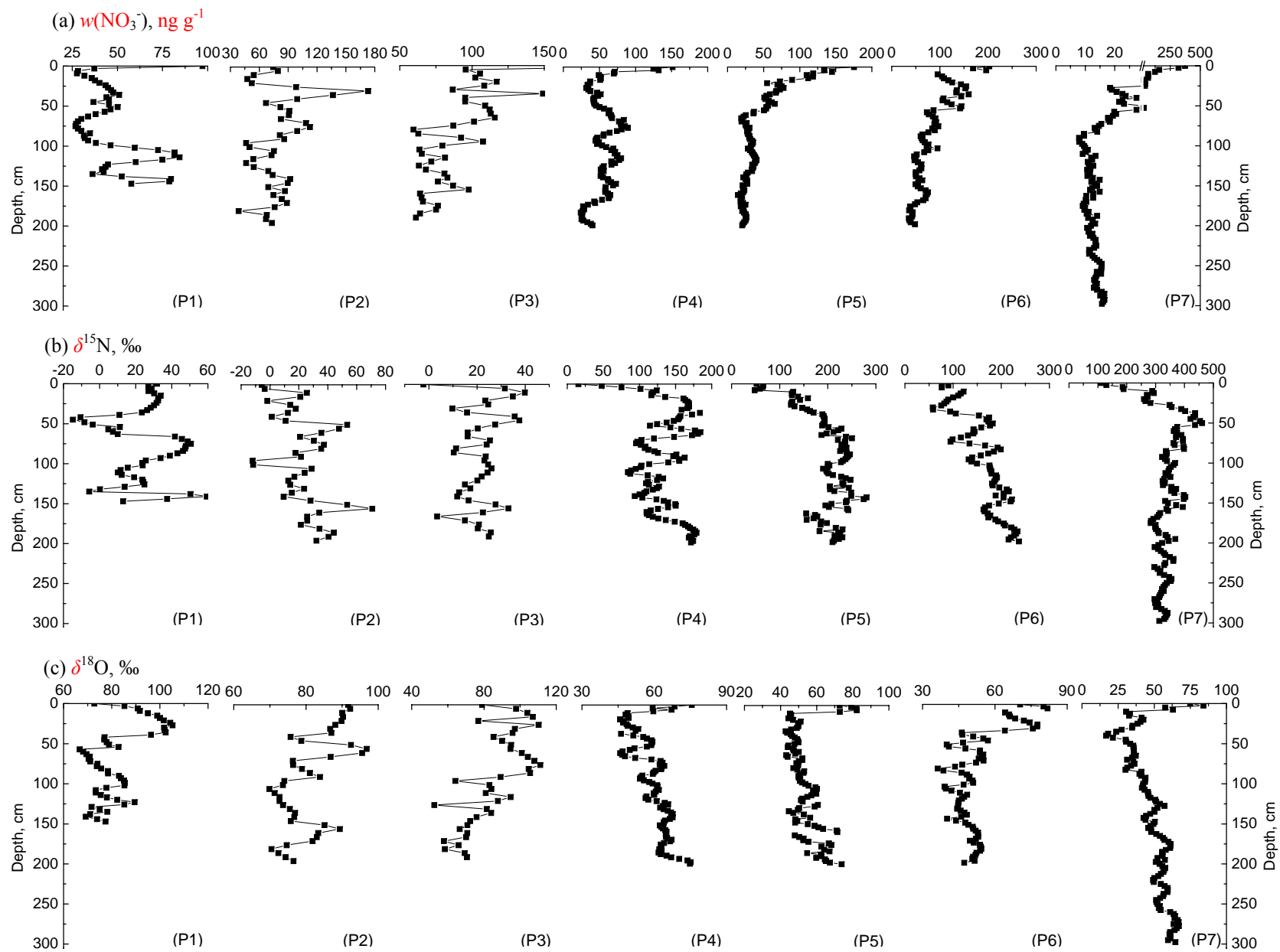


Fig. 3. Detailed profiles of $w(\text{NO}_3^-)$ (a) and isotopic composition $\delta^{15}\text{N}$ (b) and $\delta^{18}\text{O}$ of NO_3^- (c) in the P1-P7 snowpits. It is noted that the x-axis of $w(\text{NO}_3^-)$ in P7 was broken to show the trend clearly in deeper snowpack.

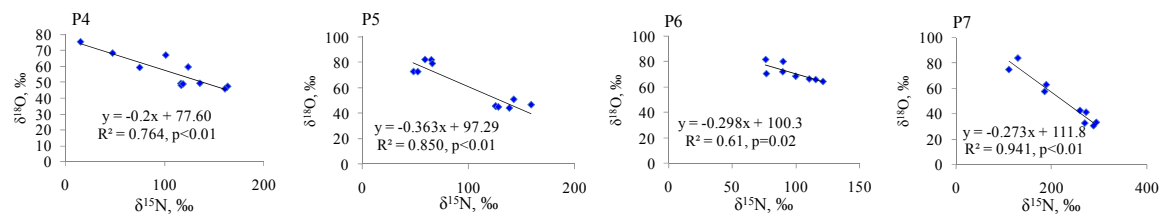


Fig. 4. Linear relationships between $\delta^{18}\text{O}$ and $\delta^{15}\text{N}$ of NO_3^- in the topmost 20 cm of the snowpits. Least squares regressions are shown and are all significant at $p < 0.05$.

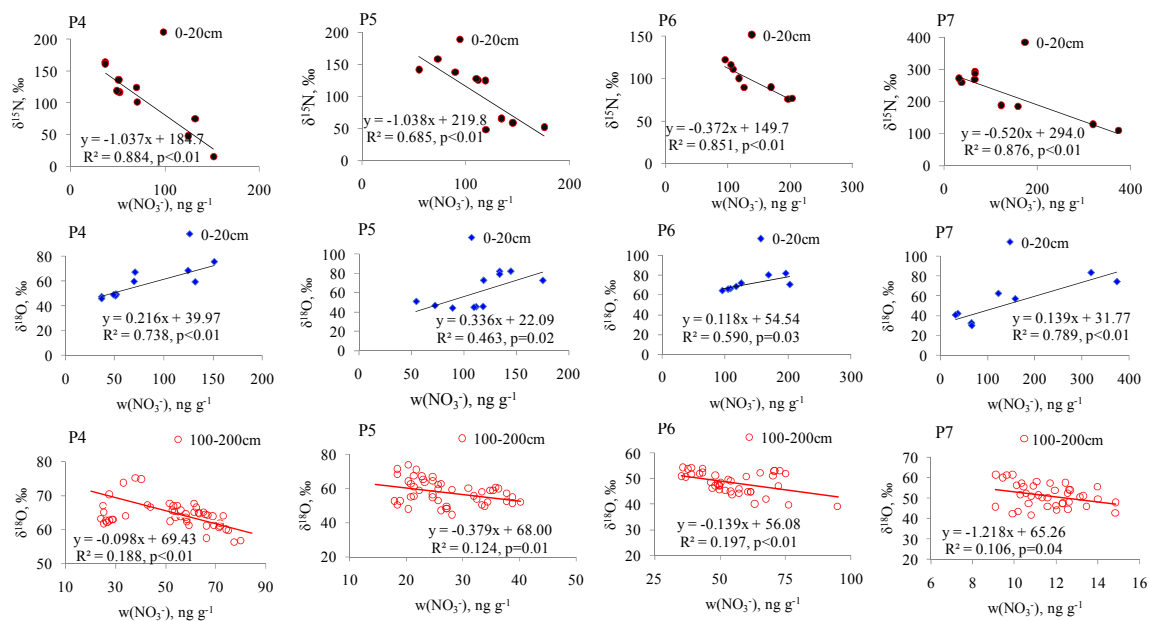


Fig. 5. Linear relationships between $w(\text{NO}_3^-)$ and $\delta^{18}\text{O}$ and $\delta^{15}\text{N}$ of NO_3^- in the near surface (top and middle rows) and at depth (bottom row) snow ranges. Least squares regressions are shown and are all significant at $p < 0.05$.

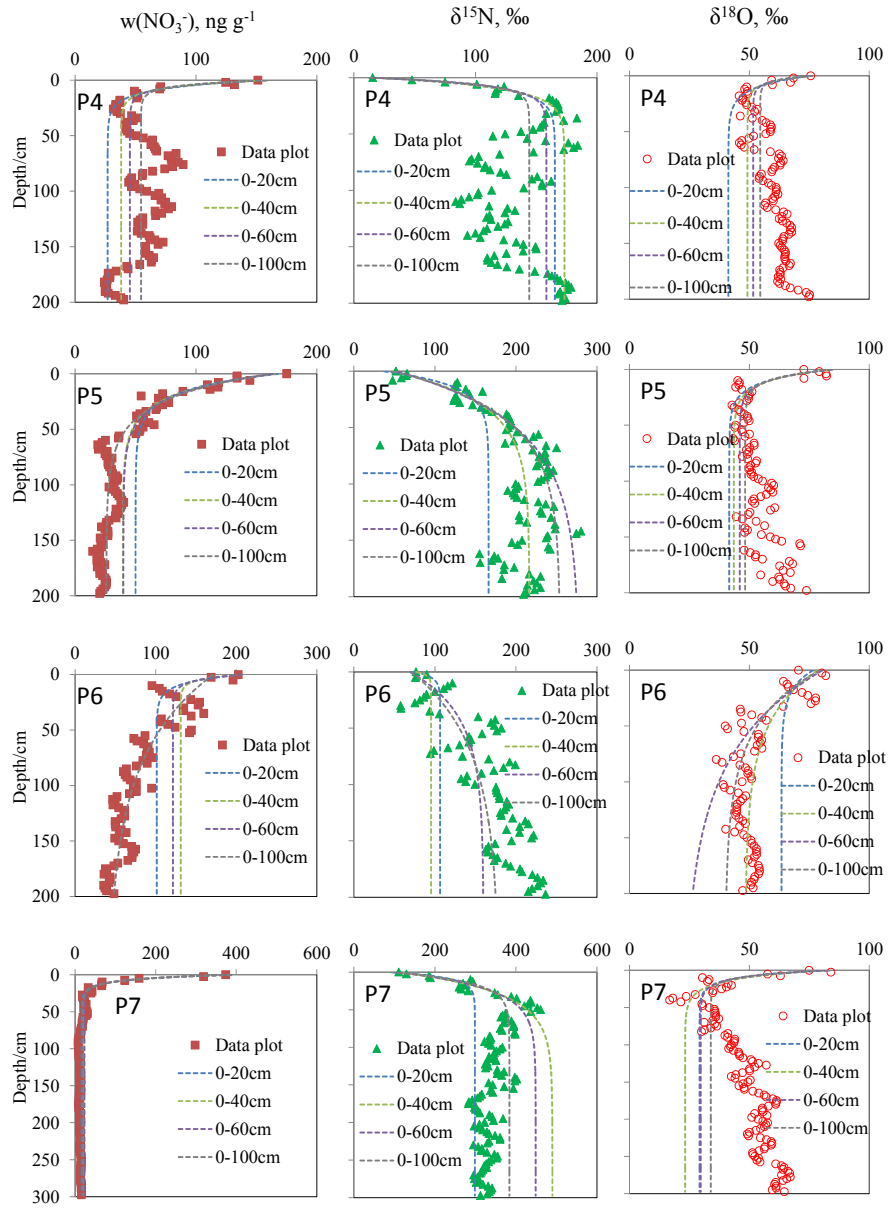


Fig. 6. Detailed profiles of $w(\text{NO}_3^-)$, $\delta^{15}\text{N}$ and $\delta^{18}\text{O}$ in different snow depth intervals (0-20cm, 0-40cm, 0-60cm, and 0-100cm) for the snowpits P4-P7. The dashed lines are the best fit regressions for the observed data, and asymptotic values are calculated for $w(\text{NO}_3^-)$, $\delta^{15}\text{N}$ and $\delta^{18}\text{O}$ by Eq. (6).

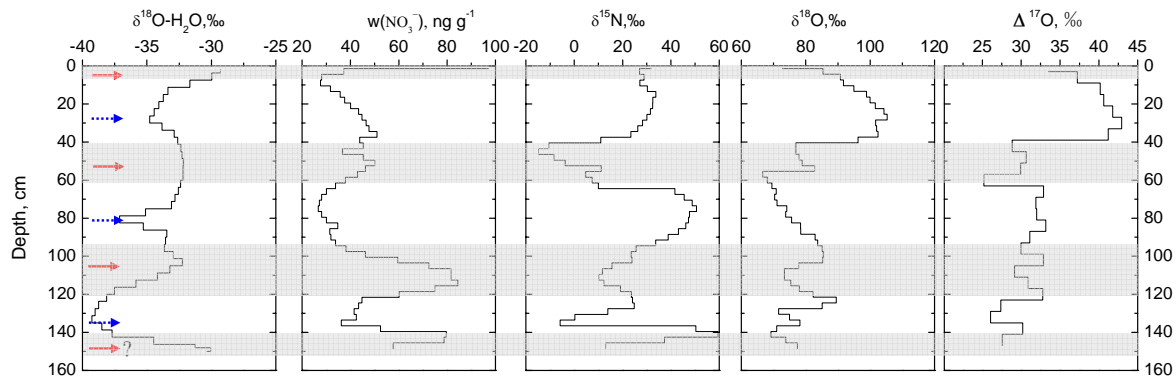


Fig. 7. Seasonality in $w(\text{NO}_3^-)$, $\delta^{15}\text{N}$, $\delta^{18}\text{O}$ and $\Delta^{17}\text{O}$ of NO_3^- in the P1 snowpit. Red solid arrows and blue dashed arrows represent the middle of the identified warm and cold seasons, respectively, and shaded areas denote warm seasons (see text). One seasonal cycle represents one $\delta^{18}\text{O}(\text{H}_2\text{O})$ peak to the next. Seasonal assignment of snow near the pit base is subject to uncertainty due to the limited coverage and absent comparison with a preceding cold season.

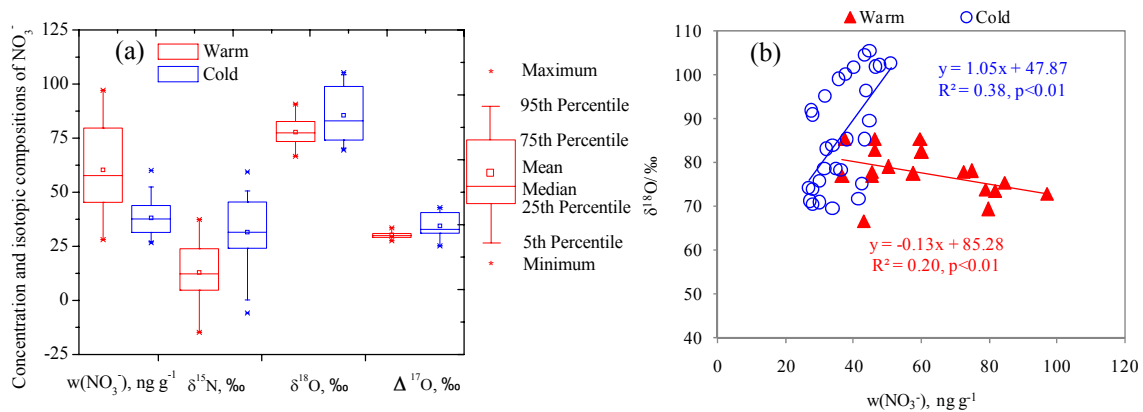


Fig. 8. $w(\text{NO}_3^-)$, $\delta^{15}\text{N}$, $\delta^{18}\text{O}$ and $\Delta^{17}\text{O}$ of NO_3^- in warm and cold season samples from snowpit P1. Summary statistics by season are shown in (a), and the seasonal relationships between $w(\text{NO}_3^-)$ and $\delta^{18}\text{O}$ of NO_3^- are shown in (b).